

# Maxwell’s Demon at Work: Efficient Pruning by Leveraging Saturation of Neurons

Simon Dufort-Labbé<sup>1</sup> Pierluca D’Oro<sup>1</sup> Evgenii Nikishin<sup>1</sup>  
Razvan Pascanu<sup>2</sup> Pierre-Luc Bacon<sup>1</sup> Aristide Baratin<sup>3</sup>

## Abstract

When training deep neural networks, the phenomenon of *dying neurons*—units that become inactive or saturated, output zero during training—has traditionally been viewed as undesirable, linked with optimization challenges, and contributing to plasticity loss in continual learning scenarios. In this paper, we reassess this phenomenon, focusing on sparsity and pruning. By systematically exploring the impact of various hyperparameter configurations on dying neurons, we unveil their potential to facilitate simple yet effective structured pruning algorithms. We introduce *Demon Pruning* (DemP), a method that controls the proliferation of dead neurons, dynamically leading to network sparsity. Achieved through a combination of noise injection on active units and a one-cycled schedule regularization strategy, DemP stands out for its simplicity and broad applicability. Experiments on CIFAR10 and ImageNet datasets demonstrate that DemP surpasses existing structured pruning techniques, showcasing superior accuracy-sparsity tradeoffs and training speedups. These findings suggest a novel perspective on dying neurons as a valuable resource for efficient model compression and optimization.

## 1. Introduction

Dying neurons, a phenomenon frequently observed during the learning process of neural networks, are traditionally viewed as detrimental, often leading to suboptimal performance (Maas et al., 2013; Xu et al., 2015) or loss of plasticity, especially in non-stationary settings (Lyle et al., 2023; Nikishin et al., 2022; Abbas et al., 2023). In response,

multiple mitigation strategies have been proposed, from alternative activation functions without a hard-saturated state—such as Leaky ReLU (Maas et al., 2013), Swish (Ramachandran et al., 2018), GELU (Hendrycks & Gimpel, 2016)—to wide use of normalization (Lyle et al., 2023) or targeted resets of weights (D’Oro et al., 2022; Dohare et al., 2021).

In this work, we revisit this phenomenon through the lens of network sparsity and pruning. Drawing on both intuitive and theoretical insights, we showcase how hyperparameter choices can encourage the saturation of units, offering an effective strategy for pruning the architecture. We introduce Demon Pruning (DemP), which combines regularization and noise injection on active units to control the proliferation of dead neurons. Drawing an analogy to Maxwell’s demon thought experiment (Maxwell, 1872) in thermodynamics, DemP leverages the asymmetry observed in the saturation process, guiding units from an active to an inactive state.

The originality of DemP lies in its active promotion of unit saturation, dynamically yielding sparser subnetworks throughout training. Its simplicity, allowing dead units to be directly identified by inspecting their activations with a few forward passes, ensures pruning at nearly no additional cost, in contrast with many existing methods (see e.g., Lee et al., 2023). Despite its simplicity, DemP achieves superior accuracy-sparsity tradeoffs when compared to strong comparable baselines like EarlyCrop (Rachwan et al., 2022) or SNAP (Verdenius et al., 2020). For instance, it outperforms by up to  $\sim 2.5\%$  beyond 80% sparsity training a ResNet-18 on CIFAR-10 or a ResNet-50 on ImageNet, coupled with a higher training speedup, reaching up to 1.23x faster on ImageNet. Finally, beyond demonstrating strong empirical performance, DemP seamlessly integrates into any training algorithm and can be readily combined with existing pruning techniques.

Our primary contributions are as follows:

1. **Insights into Neuron Saturation.** We delve into the mechanisms of saturating units, shedding light on the significant role played by stochasticity and the impact of key hyperparameters like learning rate, batch size, and regularization parameters (Sec. 2).

<sup>1</sup>Mila, Université de Montréal, Canada <sup>2</sup>Google DeepMind, London, UK <sup>3</sup>Samsung - SAIT AI Lab, Montreal, Canada. Correspondence to: Simon Dufort-Labbé <simon.dufort-labbe@mila.quebec>.

2. **A Structured Pruning Method.** Building on our insights, we present DemP, a dynamic sparsity approach that encourages a controlled proliferation of dead neurons and removes them in real-time as they arise during training, resulting in substantial training speedups (Sec. 3)
3. **Empirical Validation.** Extensive experiments on CIFAR-10 and ImageNet datasets demonstrate that DemP, despite its simplicity and versatility, surpasses strong existing structured pruning baselines in terms of accuracy-compression tradeoffs and achieves results comparable to unstructured pruning methods (Sec. 4).

## 2. Saturating Units: An Analysis

The goal of this section is to offer theoretical insights into the occurrence of dead neurons and explore the impact of different training heuristics and hyperparameters.

Given a neural network and a set of  $n$  training data samples, we denote by  $a_j^\ell \in \mathbb{R}^n$  the vector of activations of the  $j$ th neuron in layer  $\ell$  for each training input. We adopt the following definition of a *dead neuron* throughout the paper:

**Definition:** The  $j$ -th neuron in layer  $\ell$  is *inactive* if it consistently outputs zero on the entire training set, i.e.  $a_j^\ell = 0$ .<sup>1</sup> A neuron that becomes and remains inactive during training is considered as *dead*.<sup>2</sup>

Many modern architectures use activations functions with a saturation region that typically includes 0 at its boundary. In this case, when a neuron becomes inactive during training, its incoming weights also receive zero—or very small<sup>3</sup>—gradients, which makes it difficult for the neuron to recover. In this paper, we mostly work with the Rectified Linear Unit (ReLU) activation function,  $\sigma(x) = \max(0, x)$ . In this case, the activity of a neuron depends on the sign of the corresponding pre-activation feature.

### 2.1. Neurons Die During Training

We begin with some empirical observations. Applying the above criterion (Footnote 1) with threshold parameter  $\epsilon = 0.01$ , we monitor the accumulation of dead neurons during training of a Resnet-18 (He et al., 2016) on CIFAR-10 (Krizhevsky et al., 2009) with the Adam optimizer (Kingma & Ba, 2015), with various learning rates and choices of activation functions.

The outcomes are shown in Fig.1, revealing a notable and

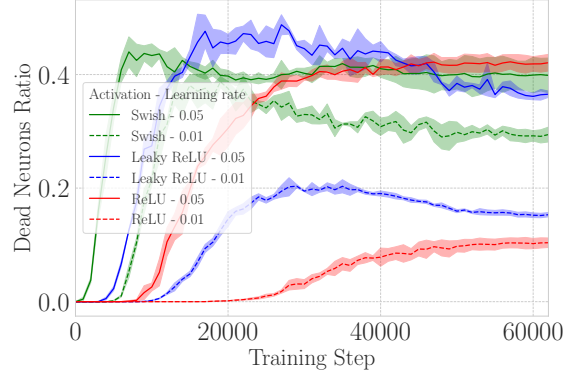


Figure 1. Dead neuron accumulation for a ResNet-18 trained on CIFAR-10 with different activation functions and values of the learning rate. We use a negative slope of  $\alpha = 0.05$  for Leaky ReLU and a  $\beta = 1$  for Swish.

sudden increase in the number of inactive neurons early in training. Moreover, a minimal portion of these inactive neurons shows signs of recovery in later stages of training (see Fig. 9 in Appendix C). Overall, this results in a significant fraction of the 3904 neurons/filters in the convolutional layers of the ResNet-18 dying during training, particularly with a high learning rate. We note that this phenomenon is not exclusive to ReLU activations.

**Intuition.** Similar to Maxwell’s demon thought experiment (Maxwell, 1872), one can picture an asymmetric behavior of how weights can move across the boundary that delimitates the saturated versus non-saturated state of a unit, akin to the demon’s selective passage of molecules. Neurons, or more specifically their weights, can move freely within the active region, but once they enter the inactive region their movement is impeded, similar to how the demon can trap molecules in a low-energy subspace. In this context, neuron death can be influenced by various factors, e.g., noise from the data, being too close to the border, or taking too large gradient steps. Once the neuron moves into the inactive zone, neurons can only be reactivated if the boundary itself shifts. This asymmetry makes it more likely for neurons to die than to revive.

We formalize this analogy with simple theoretical models in Appendix B. These models are meant to capture the multiplicative (i.e. parameter dependent) nature of the gradient noise in SGD. Multiplicative noise in stochastic processes is known to cause regions with lower noise magnitude to act as attractors (Oksendal, 2010). Essentially, lower noise regions (such as the inactive region of a saturating unit) tend to retain the system due to reduced impact, while higher noise regions push it away. We explicitly demonstrate this phenomenon in the theoretical settings of Appendix B.

<sup>1</sup> In practice, especially for non-ReLU activation functions, we will be using the notion of  $\epsilon$ -inactivity, defined by the condition  $|a_i^\ell| < \epsilon$ , for some threshold parameter  $\epsilon$ .

<sup>2</sup>For convolutional layers we treat filters as neurons (see Appendix A).

<sup>3</sup>e.g., due to regularization.

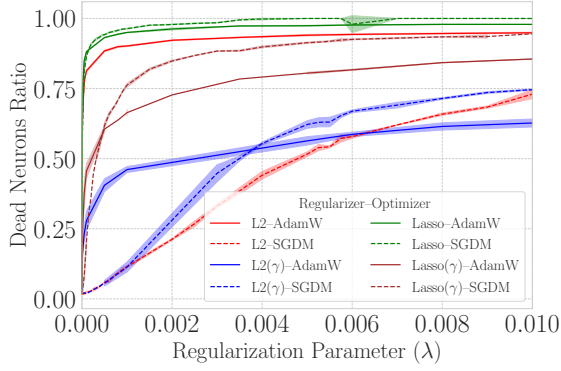


Figure 2. Increased regularization during training increases the ratio of dead units, as showcased here for a ResNet-18 trained on CIFAR-10. We use  $\cdot(\gamma)$  to denote when regularization is applied solely to the scale parameters of the normalization layers.

## 2.2. Factors Impacting Dying Ratios

**Role of regularization.** The above intuition suggests that maintaining activations close to zero increases the likelihood of neuron death, aligning them closer to the inactive region (the negative domain for ReLU networks). As illustrated in Fig. 2, training a ResNet-18 on CIFAR 10 (with Adam or SGD+momentum) with a higher L2 or Lasso regularization leads to sparser networks caused by an accumulation of dead units. Section 3 elaborates on the approach with DemP, where we opt to apply regularization exclusively on the scale parameters of the normalization layers, following Liu et al. (2017a). This tends to better preserve performance and yields significantly improved accuracy-sparsity tradeoffs, as shown in Fig 6 in Appendix F.

**Role of noise.** Our simple model suggests a pivotal role played by the noise of the training process in the occurrence of dying neurons. To investigate this in a simple setting, we train small MLPs on a subset of 10 000 images of the MNIST dataset in three different noisy regimes: vanilla SGD, pure SGD noise (obtained by isolating the noisy part of the minibatch gradient), and pure Gaussian noise. As observed in Fig. 10 in Appendix D.1, while pure SGD noise training yields dying ratios comparable to SGD, training with pure Gaussian noise is much less prone to dead neuron accumulation. We hypothesize that this difference is due to the asymmetry of SGD noise: since the gradients are 0 for dead neurons, only (the weights of) live neurons are subject to noisy updates. In contrast, the weights of inactive neurons get updated under Gaussian noise training, which increases their probability of recovery. As we spell out in Section 3, DemP injects Gaussian noise exclusively to weights of live neurons during training, which reveals effective to encourage neuron death (see Fig. 3 and Fig. 10, middle plot).

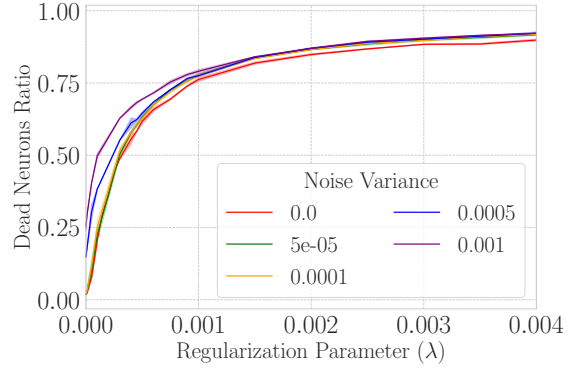


Figure 3. Augmenting training updates with asymmetric Gaussian noise, sampled from  $\mathcal{N}(x|0, \sigma^2)$  and applied to live neurons only, also leads to higher levels of dead unit accumulation, as showcased here for a ResNet-18 trained on CIFAR-10 with various values of the Lasso( $\gamma$ ) regularization parameter.

We note that other ways to control the SGD noise variance include varying the learning rate and/or the batch size. Fig. 11 (right) in Appendix D.1 illustrates how increasing the learning rate or diminishing the batch size indeed increases dying ratios. However, it proved more challenging to balance accuracy and sparsity by adjusting these hyperparameters, as they also significantly affect overall performance. Instead, DemP maintains these parameters at their default or task-optimized values, facilitating its integration into existing training routines.

**Optimizer.** We expect the choice of optimizer to affect the final count of dead neurons post-training (e.g. for adaptive optimizers, by altering the effective learning rate per parameter). Notably, we observe a significant discrepancy between using the Adam optimizer (Kingma & Ba, 2015) and SGD with momentum (SGDM) (Fig. 2). As also emphasized by Lyle et al. (2023), we attribute this difference primarily to the specific hyperparameter selection for Adam ( $\beta_1, \beta_2, \epsilon$ ), which has a substantial impact on neuron death (further discussed in Appendix E). Results from experiments with both optimizers are presented in the next section.

Finally, the total training time and network width can also impact the occurrence of dying neurons and are explored respectively in Appendix D.2 and Appendix D.3.

## 3. Demon Pruning

Leveraging insights from Sec. 2, we introduce Demon Pruning (DemP), summarized in Algorithm 1. It relies on two key elements: regularization and noise, influencing the learning dynamics to yield sparse solutions. Higher sparsity levels are achieved solely by increasing the peak regularization parameter ( $\lambda$ ), as highlighted in Fig. 2.

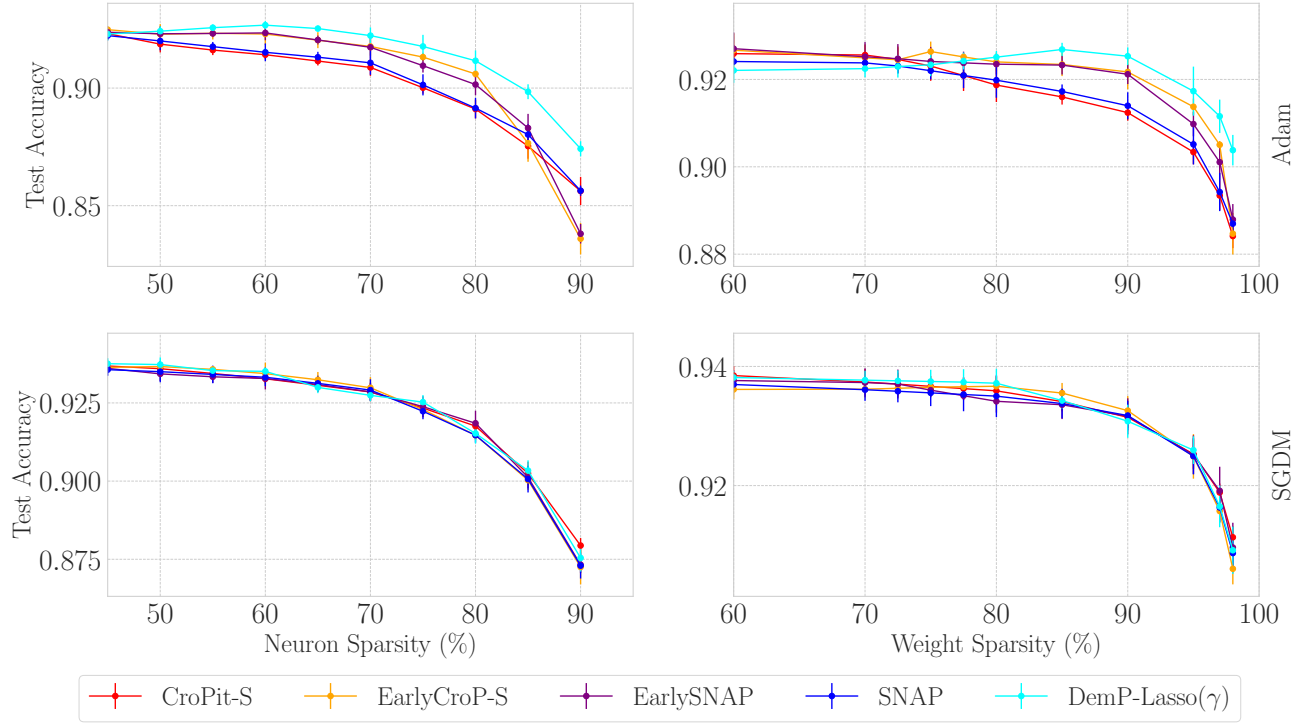


Figure 4. **Top:** For ResNet-18 networks on CIFAR-10 trained with Adam (ReLU), DemP can find sparser solutions maintaining better performance than other structured approaches. Higher sparsities with DemP are obtained by increasing the peak strength of the added scheduled regularization. **Bottom:** With SGDM, DemP performance is on par, without significant differences between methods. **Left:** Neural sparsity, structured methods. **Right:** Weight sparsity, structured methods.

#### Algorithm 1 DemP Algorithm

**Input:** Learning rate  $\eta$ , pruning frequency  $\tau$ , regularization parameter  $\lambda$ , noise variance  $\sigma^2$ , subset of parameters with added scheduled regularization  $\gamma$

**Initialize:** Weights  $w_0$ , schedules  $S_\lambda(t)$  and  $S_\sigma(t)$

**for**  $t = 0$  to  $T$  **do**

    Compute gradient:  $\nabla L(w_t)$

    Update  $\lambda_t$  and  $\sigma_t^2$ :

$\lambda_t \leftarrow S_\lambda(t)$

$\sigma_t^2 \leftarrow S_\sigma(t)$

    Regularization term:  $\nabla R(\gamma, \lambda_t)$

    Sample asymmetric noise:  $\xi_{\text{asym}} \sim \mathcal{N}(0, \sigma_t^2)$

    Update weights:

$w_{t+1} \leftarrow w_t - \eta(\nabla L(w_t) + \nabla R(\gamma, \lambda_t)) + \xi_{\text{asym}}$

**if**  $t \% \tau = 0$  **then**

        Remove dead neurons

**end if**

**end for**

**Regularization ( $R(\gamma, \lambda)$ ):** Looking at the pre-activations ( $\hat{z}^{[l]}$ ) after batch normalization of the output of layer  $l$  ( $\mathbf{F}_l(\mathbf{W}^{[l]}, \mathbf{a}^{[l-1]})$ )

$$\hat{z}^{[l]} = \gamma^{[l]} \odot \left( \frac{\mathbf{F}_l(\mathbf{W}^{[l]}, \mathbf{a}^{[l-1]}) - \mu^{[l]}}{\sqrt{\sigma^{2[l]} + \epsilon}} \right) + \beta^{[l]} \quad (2)$$

hints toward two strategies to push  $\hat{z}^{[l]}$  toward zero: **1.** regularizing all networks parameters, **2.** regularizing the scale normalization parameters ( $\gamma$ ). We refrain from regularizing the offset parameters ( $\beta$ ) because negative offsets can help to drive the pre-activations into the negative region. Our method by default uses Lasso regularization on scale parameters of normalization layers, as in Liu et al. (2017a). Without normalization, weight regularization serves as an alternative to encourage sparsity (Fig. 2).

Based on the insights of the previous section, we use a one-cycled schedule (Smith & Topin, 2018) regularization strategy with minimal impacts:

- Because neurons die early in training (see 2.1), regularization can be gradually decayed, allowing the network to recover some expressivity.
- Previous works showcased that it can be beneficial to prune at an early stage instead of at initialization

Specifically, DemP updates parameters in the form:

$$w_{t+1} = w_t - \eta(\nabla L(w_t) + \nabla R(\gamma, \lambda)) + \xi_{\text{asym}} \quad (1)$$

where  $\nabla L(w_t)$  denotes the gradient estimator of some base optimizer, and  $R(\gamma, \lambda)$  and  $\xi_{\text{asym}}$  are regularization and noise terms defined below.



(Frankle et al., 2020; Rachwan et al., 2022). With our approach, this can be achieved by using warmup.

Employing a one-cycle strategy (Smith & Topin, 2018) effectively exploits the advantages of both warmup and decay phases. We illustrate the robustness of our design choices in the extensive ablation analysis in Sec. 4.3.

**Asymmetric noise ( $\xi_{\text{asym}}$ ):** Sec. 2.2 and Appendix B illustrate how SGD noise’s asymmetry aids in driving neurons towards inactivity by dissipating as they become inactive. DemP mimics this effect by injecting artificial noise exclusively into the weights of active units. Adding low variance Gaussian noise  $\chi \sim \mathcal{N}(x|0, \sigma^2)$  to the updates of active unit weights enhances sparsity without impacting performance (see Fig. 7). The relevance of injecting artificial noise is further justified in Fig. 13 where we show that it is by itself a sound strategy to sparsify neural networks, even in the absence of regularization.

DemP thus introduces two novel hyperparameters: growing regularization on normalization scaling and artificial noise. Notably, this addition does not affect standard hyperparameters, such as weight decay, maintaining DemP’s compatibility with existing training methodologies. By retaining this orthogonality, DemP seamlessly integrates into various training setups without any additional overhead. Furthermore, this approach allows for more extensive exploration of other hyperparameters to achieve sparser solutions.

## 4. Empirical Evaluation

Through extensive empirical evaluation across various benchmarks, we consistently observe that DemP achieves superior performance/sparsity tradeoffs, particularly at high sparsity levels and when combined with Adam.

### 4.1. Setup

We focus our experiments on computer vision tasks, which is standard in pruning literature (Gale et al., 2019). We train ResNet-18 and VGG-16 networks on CIFAR-10, and ResNet-50 networks on ImageNet (He et al., 2016; Simonyan & Zisserman, 2015; Krizhevsky et al., 2009; Deng et al., 2009). We follow the training regimes from Evci et al. (2020) for ResNet architectures and use a setting similar to Rachwan et al. (2022) for the VGG to broaden the scope of our experiments. The results for pruning the VGG are reported in Appendix G and training details are provided in Appendix H.

Our method is a structured pruning method, removing entire neurons at once, and pruning happens during training, transitioning from a dense network to a sparse one. The methods we compare with follow this paradigm, except for

Table 1. Comparison between different criteria when pruning a ResNet-50 trained on ImageNet with Adam around 80% (first line) and 90% (second line) weight sparsity. **DemP improves test accuracy by 2.85% and 2.14%** at those respective sparsities over the strongest baselines. Because structured pruning methods do not have precise control of weight sparsity, we report the closest numbers obtained to these target values.  $\pm$  indicates the standard deviation, computed from 3 seeds. The sparsity numbers indicate the removed ratio.

	Method	Test accuracy	Neuron sparsity	Weight sparsity
	Dense	74.98% $\pm 0.08$	-	-
Structured Methods	SNAP	28.28% $\pm 0.08$	36.9%	81.4%
		27.17% $\pm 0.07$	56.0%	90.1%
	CroPit-S	28.34% $\pm 0.52$	36.9%	81.4%
		27.36% $\pm 0.16$	53.2%	89.9%
	EarlySNAP	68.67% $\pm 0.15$	51.70%	80.37%
		63.80% $\pm 0.58$	66.6%	90.06%
	EarlyCroP-S	68.26% $\pm 0.31$	51.60%	79.97%
		64.20% $\pm 0.27$	66.6%	90.37%
	DemP-L2	71.52% $\pm 0.09$	61.83%	80.13%
		66.34% $\pm 0.16$	74.1%	89.93%

Table 2. Speedups and computational gains for the ResNet-50 model trained on ImageNet with Adam around 80%/90% weight sparsity, computed from 3 seeds. While SNAP and CroPit-S achieve better speedup, they do so by dropping significantly the test accuracy below 30%. DemP achieves much better speedups compared with EarlySNAP and EarlyCroP-S which maintain accuracy above 60%

Method	Training time	Training FLOPs	Inference FLOPs
Dense	1.0x	1.0x (3.15e18)	1.0x (8.2e9)
SNAP	0.51x/0.48x	0.32x/0.25x	0.32x/0.25x
CroPit-S	0.52x/0.47x	0.32x/0.27x	0.32x/0.27x
EarlySNAP	0.95x/0.75x	0.63x/0.46x	0.63x/0.45x
EarlyCroP-S	0.94x/0.82x	0.66x/0.51x	0.66x/0.50x
DemP-L2	0.81x/0.61x	0.57x/0.42x	0.49x/0.34x

approaches like Lasby et al. (2023), which achieves remarkable performance but primarily relies on unstructured pruning followed by structured reorganization. We employ the following structured pruning baselines: Crop-it/EarlyCrop (Rachwan et al., 2022), SNAP (Verdenius et al., 2020) and a modified version using the early pruning strategy from Rachwan et al. (2022) (identified as EarlySNAP). We trained these baselines using the recommended configuration of the original authors; in particular, we did not subject them to the regularization schedule employed by our method.

## 4.2. Results

DemP demonstrated superior performance when paired with Adam optimizer, consistently outperforming all baselines at high sparsity across the board. The margin in test error can reach up to 2.25% when training on CIFAR-10 and ImageNet (Fig. 4, 15 and Table 1). The results are more contrasted with SGDM: DemP performs similarly to baselines on ResNet-18 benchmarks (see Fig. 4, 15), is outperformed at higher sparsities on VGG (see Fig. 14) but slightly outperforms baselines when training a ResNet-50 on ImageNet (refer to Table 3). Additionally, DemP provides significant speedup when training on Imagenet with both optimizers, surpassing baselines yet again (Table 2 and 3).

Furthermore, as shown in Fig. 15, these conclusions hold when a ResNet-18 is trained with Leaky ReLU activations instead of ReLU, highlighting DemP’s flexibility across different activations functions.

## 4.3. Ablation

**Regularizers.** While the methodology works with both L2 and Lasso regularization, and either over the entire parameter space or specifically to the scale normalization parameters ( $\gamma$ ), we empirically found that Lasso regularization of the scaling worked best for SGDM (Fig 6). For Adam, L2 regularization of the scaling slightly outperforms Lasso regularization of the scaling (Fig 6). As such, normalizing solely the scale parameters is beneficial to performance. For simplicity, we opted for Lasso regularization of the scale parameters in all subsequent experiments. Nevertheless, in the absence of normalization layers, traditional regularization methods remain viable for inducing sparsity in the model

**Dynamic Pruning.** To realize computational gain during training, we prune dynamically the NN at every  $k$  steps (with a default of  $k = 1000$ ). Dead neurons end up removed almost as they appear, not giving them any chance to be revived. This strategy allows to speed up the training with no significant change in performance as shown in Fig. 8. We note that this smooth gradual pruning process is compatible with our approach in part because there is no added cost for computing the pruning criterion.

**Dead Criterion Relaxation.** The definition we choose for a dead neuron asks for it to be inactive to the entire dataset. In practice, we found that this criterion could be relaxed and defaulted to using 512 (2048 for ImageNet) examples from the training dataset to measure the death state (measuring across multiple minibatches when necessary). Fig. 12 shows that using this proxy for tracking dead units is sufficient. Pruning interventions become highly efficient, incurring only the computational cost of a few forward propagation batches.

**Regularization Schedule.** We test our hypotheses about

regularization scheduling by comparing the one-cycle method with warmup, cosine decay, and constant schedules. Empirically, we confirm in Fig. 5 that using a one-cycle scheduler for the regularization parameter ( $\lambda$ ) is a good strategy (Appendix F.4).

**Added noise.** Adding asymmetric noise is particularly beneficial to further increase sparsity (see Fig. 7). The noise is kept small, with a peak variance at  $\sigma^2 = 5 \times 10^{-5}$  and following the same schedule as the added regularization for maximal effect. We believe it acts as the small additional push helping neurons lingering close to the inactive region boundary to cross it.

We conducted experiments to assess the necessity of using asymmetric noise in DemP (refer to Fig. 13). Surprisingly, we found that when all other aspects of DemP remained constant (including dynamic pruning), asymmetric noise was not essential. We yet decided to keep the added noise asymmetric due to significant differences observed in other settings (Fig. 10, middle) where the impact of symmetric noise on dead neuron accumulation was considerably less pronounced due to neuron revival.

**Weight Decay.** Our method defaults back to traditional regularization, with a term added directly to the loss, as opposed to the weight decay scheme proposed by Loshchilov & Hutter (2019). By doing so, the adaptive term in optimizers takes into account regularization, and neurons move more quickly toward the inactive region. From a pruning perspective, it achieves a higher sparsity than weight decay for the same regularization strength.

**Activation function.** Dead neurons, and thus the pruning mechanism behind our method, are naturally defined with ReLU activation functions, in which neurons can completely deactivate. However, multiple activation functions, such as Leaky ReLU (Maas et al., 2013), also exhibit a “soft” saturated region. We postulate that neurons firing solely from the saturated region do not contribute much to the predictions and can be considered *almost dead*. We test this hypothesis by employing our method in a network with Leaky ReLU activations (Fig. 15), removing neurons with only negative activation across a large minibatch. Again, our method can outperform other structured methods when using Adam and offers a similar performance with SGDM.

## 5. Related Works

While our method monitors activations (Hu et al., 2016) and leverages increasing regularization (Wang et al., 2021) on scale parameters (Liu et al., 2017a), DemP introduces new techniques for pruning, beginning with the artificial asymmetric noise injected during optimization to further promote sparsity (Eq. 1.) Also, with DemP, sparsity naturally arises from the learning dynamics, removing the need for defining

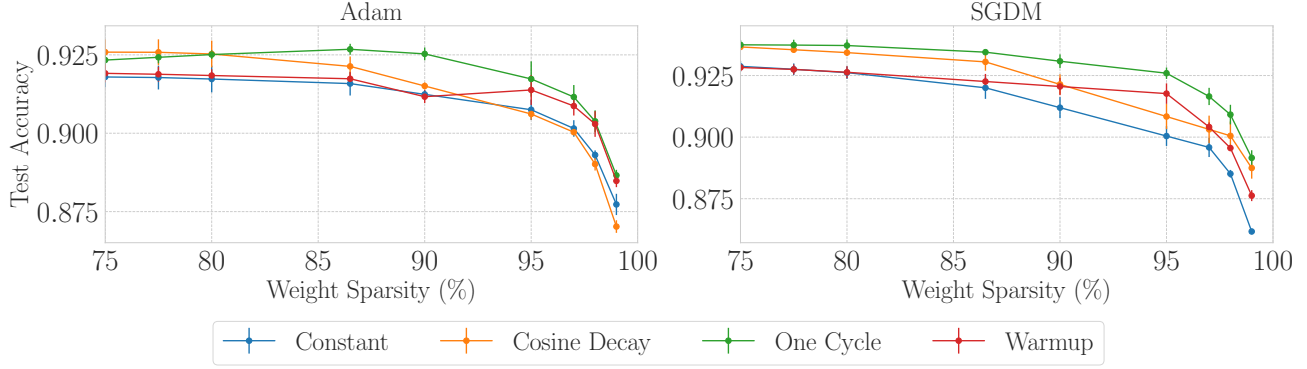


Figure 5. We studied the impact of different schedules over the regularization parameter for our method, settling down on a one-cycle scheduler as default. Experiments were performed with ResNet-18 on CIFAR-10, with Lasso( $\gamma$ ) regularization, across 3 seeds. Higher sparsities are obtained by increasing the peak strength of the added scheduled regularization. **Left:** With Adam optimizer. **Right:** With SGDM optimizer.

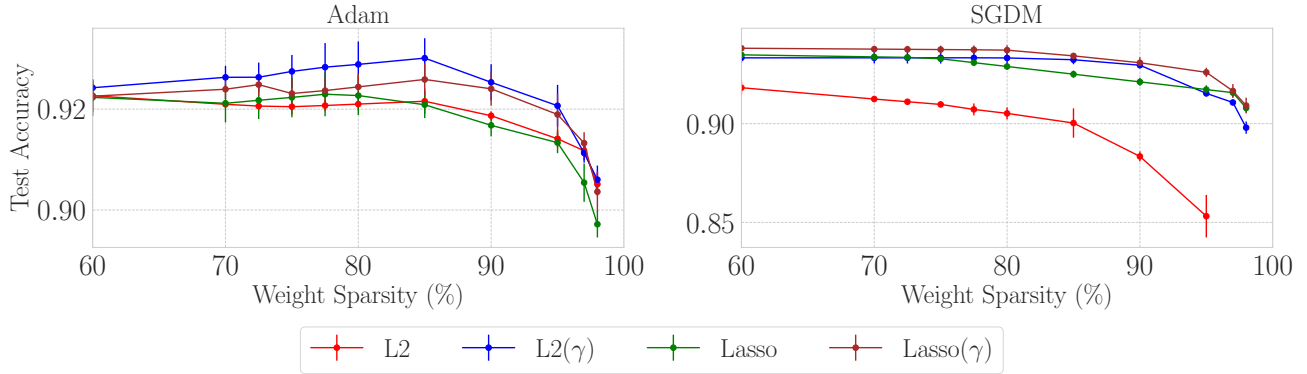


Figure 6. ResNet-18 networks trained on CIFAR-10 with different added regularization strategies, over 3 seeds.  $\cdot(\gamma)$  denotes when regularization is only applied on the scale parameters of the normalization layer. Higher sparsities are obtained by increasing the peak strength of the added scheduled regularization. **Left:** With Adam, using L2( $\gamma$ ) regularization slightly outperforms other strategies. **Right:** Using SGDM, the differences in performance become more pronounced, with Lasso regularization applied to scale parameters offering the optimal balance between sparsity and performance.

pruning criteria and the need for discrete pruning interventions impacting training. Non-contributing neurons can be promptly pruned as they become inactive, without compromising the model’s present or future performance (as illustrated in Fig. 8). Recent unstructured pruning approaches manually tailor sparsity distribution across layers (Mocanu et al., 2018; Evci et al., 2020), while structured pruning mostly rely on uniform layer-wise pruning (Rachwan et al., 2022). DemP alleviates this by letting the learning dynamics dictate the sparsity distribution across layers.

DemP eliminates the need for meticulous pruning timing (Wang et al., 2021; Rachwan et al., 2022) or the creation of a heuristic-based pruning schedule (Lee et al., 2023). Acknowledging that very early pruning can be detrimental (Frankle et al., 2020; Rachwan et al., 2022), DemP employs easy-to-tune regularization schedules to influence when units die. Iterative pruning (Verdenius et al., 2020) during a single intervention is also unnecessary, again be-

cause units die gradually during the early training phase with DemP.

**Structured Pruning.** Pruning is used to reduce the size and complexity of neural networks by removing redundant or less important elements, be they neurons or weights while maintaining their performance (LeCun et al., 1989). Recent advances such as those based on the Lottery Ticket Hypothesis (Frankle & Carbin, 2019) have demonstrated the existence of subnetworks trainable to comparable performance as their dense counterpart but with fewer parameters.

DemP is a *structured pruning* method that aims to remove entire structures within a network, such as channels, filters, or layers. It results in smaller and faster models that maintain compatibility with existing hardware accelerators and software libraries (Wen et al., 2016; Li et al., 2017). We highlight and benchmark against strong baselines that use criteria based on gradient flow to evaluate which nodes to

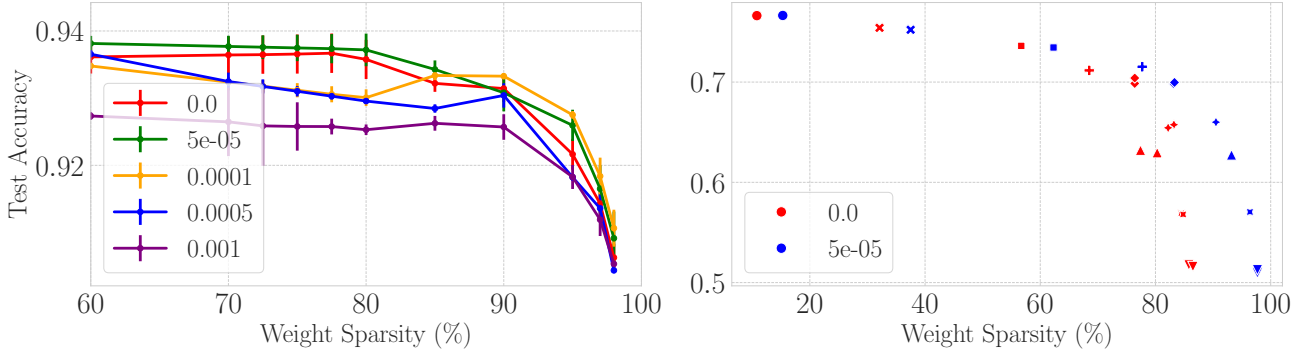


**Figure 7. Left:** ResNet-18 networks trained on CIFAR-10 with SGDM over 3 seeds. Adding a very small amount of Gaussian noise ( $\sigma^2 = 5 \times 10^{-5}$ ) to the live neurons provides the best tradeoff—performance is improved or maintained across all sparsity ratios. **Right:** The addition of noise proves very impactful in increasing sparsity without affecting performance on a ResNet-50 train on ImageNet. Each symbol represents a distinct peak regularization value for scale parameters, with one data point corresponding to each seed.

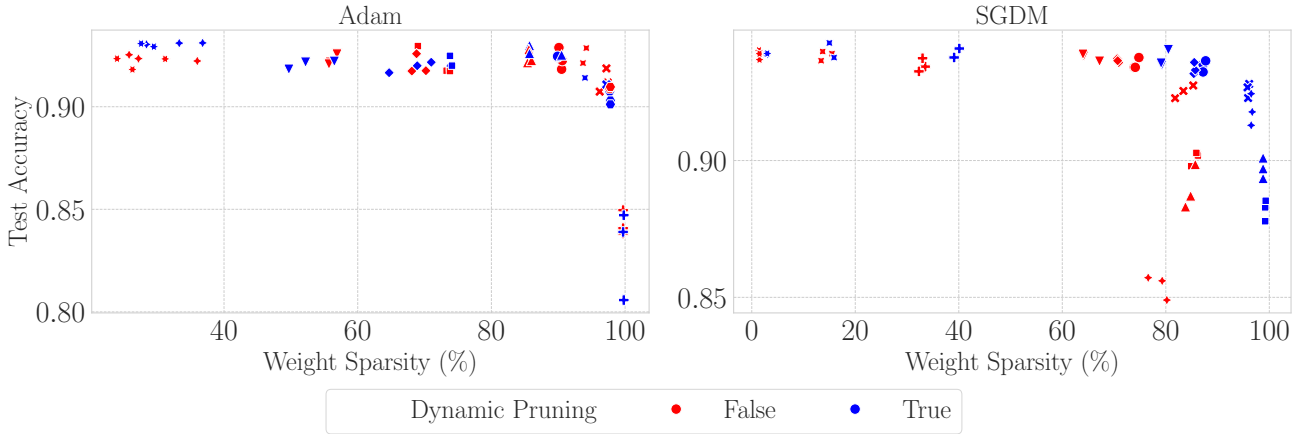


**Figure 8.** Measuring final accuracy vs. sparsity when dynamic pruning is enabled or not. Different symbols were associated with different regularization strengths. Experiments were performed with ResNet-18 on CIFAR-10 and Lasso( $\gamma$ ) regularization for 3 seeds. **Left:** With Adam, there are barely any variations between the two strategies, allowing us to conclude that using dynamic pruning does not affect performance. **Right:** With SGDM, there is a gap in sparsity, but very little variation in performance. This also makes dynamic pruning an effective tool to achieve better sparsity tradeoffs with SGDM, in addition to training speedup.

prune (Verdenius et al., 2020; Wang et al., 2020; Rachwan et al., 2022). Other works employed either L0 or L1 regularization on gate parameters (or batch normalization scaling parameters) to enforce sparsity (Liu et al., 2017b; Louizos et al., 2018; You et al., 2019), but we do not benchmark them as they are outperformed by Rachwan et al. (2022).

Regularization-based pruning has been a popular approach, with canonical papers employing L0 or L1 regularization to induce sparsity directly (Louizos et al., 2018; Liu et al., 2017b; Ye et al., 2018) while L2 can help identify the connections to prune with the smallest weight criterion (Han et al., 2015). Because uniform regularization can quickly degrade performance (Wen et al., 2016; Lebedev & Lempitsky, 2016), Ding et al. (2018) and (Wang et al., 2019) proposed to adapt the regularization for different parameter groups. Recently, Wang et al. (2021) showed that growing the L2 regularization can leverage Hessian information to

identify the filters to prune in pre-trained networks.

**Dead Neurons.** It is widely recognized that neurons, especially in ReLU networks, can saturate during training (Agarap, 2018; Trottier et al., 2017; Lu et al., 2019). In particular, Evci (2018) noted the connection of the dying rate with the learning rate and derived a pruning technique from it.

Mirzadeh et al. (2023), contemporary to our work, highlighted the strategic use of ReLU activations to achieve inference efficiency in transformer-based models. They propose an approach leveraging post-activation sparsity to improve inference speed in large language models.

Dead neurons are also studied in continual and reinforcement learning through the lens of *plasticity loss* (Berariu et al., 2021; Lyle et al., 2022), that progressively makes a model less capable of adapting to new tasks (Kirkpatrick



et al., 2016). In some scenarios, a cause of plasticity loss has been attributed to the accumulation of dead units (Sokar et al., 2023; Lyle et al., 2023; Abbas et al., 2023; Dohare et al., 2021).

## 6. Conclusion

In this work, we have explored how various hyperparameter configurations like the learning rate, batch size, regularization, architecture, and optimizer choices, collectively influence activation sparsity during neural network training. Leveraging this, we introduced Demon Pruning, a dynamic pruning method that controls the proliferation of saturated neurons during training through a combination of regularization and noise injection. Extensive empirical analysis on CIFAR 10 and ImageNet demonstrated superior performance compared to strong structured pruning baselines.

The simplicity of our approach allows for versatile adaptation. For settings requiring predefined sparsity levels, we can gradually increase regularization until reaching the target ratio. Furthermore, integrating our method with existing pruning techniques is straightforward. Employing multiple pruning criteria can enhance parameter identification for dead neurons, especially in unstructured methods leveraging increased structural sparsity from higher regularization.

Our experiments with Leaky ReLU illustrate the compatibility of our approach with activation functions featuring softer saturation regions than ReLU. This extends the applicability of our method to a broad range of models, offering a practical and accessible solution. Given the current trend of expanding model sizes, widespread adoption of our methodology could yield significant computational and environmental benefits.

## Impact Statement

Structured pruning methods, even without specialized sparse computation primitives (Elsen et al., 2020; Gale et al., 2020), can efficiently leverage GPU hardware (Wen et al., 2016) compared to unstructured methods, which is crucial as deep learning models grow and environmental impacts escalate (Strubell et al., 2019; Lacoste et al., 2019; Henderson et al., 2020). Developing energy-efficient methods that can be widely adopted is essential.

However, while efforts to enhance the efficiency of deep learning training processes can reduce computational costs and energy requirements, they may inadvertently amplify concerns associated with the rapid advancement of AI. The swift progress in AI capabilities raises significant risks, from ethical dilemmas to information manipulation. By accelerating AI development and increasing its accessibility, research like ours may exacerbate ongoing issues.

## References

- Abbas, Z., Zhao, R., Modayil, J., et al. Loss of plasticity in continual deep reinforcement learning. *CoRR*, abs/2303.07507, 2023.
- Agarap, A. F. Deep learning using rectified linear units (relu). *CoRR*, abs/1803.08375, 2018.
- Agarwal, N., Anil, R., Hazan, E., et al. Disentangling adaptive gradient methods from learning rates. *CoRR*, abs/2002.11803, 2020.
- Anderson, R. W. Chapter 7 - biased random-walk learning: A neurobiological correlate to trial-and-error. In *Neural Networks and Pattern Recognition*, pp. 221–244. Academic Press, San Diego, 1998.
- Berariu, T., Czarnecki, W., De, S., et al. A study on the plasticity of neural networks. *arXiv preprint arXiv:2106.00042*, 2021.
- Bradbury, J., Frostig, R., Hawkins, P., et al. JAX: composable transformations of Python+NumPy programs, 2018.
- Cheng, X., Yin, D., Bartlett, P., et al. Stochastic gradient and Langevin processes. In *Proceedings of the 37th International Conference on Machine Learning*, volume 119 of *Proceedings of Machine Learning Research*, pp. 1810–1819. PMLR, 13–18 Jul 2020.
- Deng, J., Dong, W., Socher, R., et al. Imagenet: A large-scale hierarchical image database. In *2009 IEEE Computer Society Conference on Computer Vision and Pattern Recognition (CVPR 2009)*, 20-25 June 2009, Miami, Florida, USA, pp. 248–255. IEEE Computer Society, 2009.
- Ding, X., Ding, G., Han, J., et al. Auto-balanced filter pruning for efficient convolutional neural networks. In *Proceedings of the Thirty-Second AAAI Conference on Artificial Intelligence, (AAAI-18), the 30th innovative Applications of Artificial Intelligence (IAAI-18), and the 8th AAAI Symposium on Educational Advances in Artificial Intelligence (EAAI-18), New Orleans, Louisiana, USA, February 2-7, 2018*, pp. 6797–6804. AAAI Press, 2018.
- Dohare, S., Mahmood, A. R., and Sutton, R. S. Continual backprop: Stochastic gradient descent with persistent randomness. *CoRR*, abs/2108.06325, 2021.
- D’Oro, P., Schwarzer, M., Nikishin, E., et al. Sample-efficient reinforcement learning by breaking the replay ratio barrier. In *The Eleventh International Conference on Learning Representations*, 2022.
- Elsen, E., Dukhan, M., Gale, T., et al. Fast sparse convnets. In *Proceedings of the IEEE/CVF conference on computer vision and pattern recognition*, pp. 14629–14638, 2020.

- Evci, U. Detecting dead weights and units in neural networks. *CoRR*, abs/1806.06068, 2018.
- Evci, U., Gale, T., Menick, J., et al. Rigging the lottery: Making all tickets winners. In *Proceedings of the 37th International Conference on Machine Learning, ICML 2020, 13-18 July 2020, Virtual Event*, volume 119 of *Proceedings of Machine Learning Research*, pp. 2943–2952. PMLR, 2020.
- Frankle, J. and Carbin, M. The lottery ticket hypothesis: Finding sparse, trainable neural networks. In *7th International Conference on Learning Representations, ICLR 2019, New Orleans, LA, USA, May 6-9, 2019*, 2019.
- Frankle, J., Dziugaite, G. K., Roy, D. M., et al. Linear mode connectivity and the lottery ticket hypothesis. In *Proceedings of the 37th International Conference on Machine Learning, ICML 2020, 13-18 July 2020, Virtual Event*, volume 119 of *Proceedings of Machine Learning Research*, pp. 3259–3269. PMLR, 2020.
- Gale, T., Elsen, E., and Hooker, S. The state of sparsity in deep neural networks. *CoRR*, abs/1902.09574, 2019.
- Gale, T., Zaharia, M., Young, C., et al. Sparse gpu kernels for deep learning. In *SC20: International Conference for High Performance Computing, Networking, Storage and Analysis*, pp. 1–14. IEEE, 2020.
- Goyal, P., Dollár, P., Girshick, R. B., et al. Accurate, large minibatch SGD: training imagenet in 1 hour. *CoRR*, abs/1706.02677, 2017.
- Han, S., Pool, J., Tran, J., et al. Learning both weights and connections for efficient neural network. In *Advances in Neural Information Processing Systems 28: Annual Conference on Neural Information Processing Systems 2015, December 7-12, 2015, Montreal, Quebec, Canada*, pp. 1135–1143, 2015.
- He, F., Liu, T., and Tao, D. Control batch size and learning rate to generalize well: Theoretical and empirical evidence. In *Advances in Neural Information Processing Systems 32: Annual Conference on Neural Information Processing Systems 2019, NeurIPS 2019, December 8-14, 2019, Vancouver, BC, Canada*, pp. 1141–1150, 2019.
- He, K., Zhang, X., Ren, S., et al. Deep residual learning for image recognition. In *2016 IEEE Conference on Computer Vision and Pattern Recognition, CVPR 2016, Las Vegas, NV, USA, June 27-30, 2016*, pp. 770–778. IEEE Computer Society, 2016.
- Henderson, P., Hu, J., Romoff, J., et al. Towards the systematic reporting of the energy and carbon footprints of machine learning. *The Journal of Machine Learning Research*, 21(1):10039–10081, 2020.
- Hendrycks, D. and Gimpel, K. Bridging nonlinearities and stochastic regularizers with gaussian error linear units. *CoRR*, abs/1606.08415, 2016.
- Hessel, M., Modayil, J., van Hasselt, H., et al. Rainbow: Combining improvements in deep reinforcement learning. In *Proceedings of the Thirty-Second AAAI Conference on Artificial Intelligence, (AAAI-18), New Orleans, Louisiana, USA, February 2-7, 2018*, pp. 3215–3222. AAAI Press, 2018.
- Hu, H., Peng, R., Tai, Y., et al. Network trimming: A data-driven neuron pruning approach towards efficient deep architectures. *CoRR*, abs/1607.03250, 2016.
- Karatzas, I. and Shreve, S. E. Brownian motion and stochastic calculus. Springer New York, NY, 2014.
- Keskar, N. S., Mudigere, D., Nocedal, J., et al. On large-batch training for deep learning: Generalization gap and sharp minima. In *5th International Conference on Learning Representations, ICLR 2017, Toulon, France, April 24-26, 2017, Conference Track Proceedings*, 2017.
- Kingma, D. P. and Ba, J. Adam: A method for stochastic optimization. In *3rd International Conference on Learning Representations, ICLR 2015, San Diego, CA, USA, May 7-9, 2015, Conference Track Proceedings*, 2015.
- Kirkpatrick, J., Pascanu, R., Rabinowitz, N. C., et al. Overcoming catastrophic forgetting in neural networks. *CoRR*, abs/1612.00796, 2016.
- Krizhevsky, A., Hinton, G., et al. Learning multiple layers of features from tiny images. 2009.
- Lacoste, A., Luccioni, A., Schmidt, V., et al. Quantifying the carbon emissions of machine learning. *CoRR*, abs/1910.09700, 2019.
- Lasby, M., Golubeva, A., Evci, U., et al. Dynamic sparse training with structured sparsity. *CoRR*, abs/2305.02299, 2023.
- Lawler, G. *Introduction to Stochastic Calculus with Applications*. Taylor & Francis, 2016.
- Lebedev, V. and Lempitsky, V. S. Fast convnets using group-wise brain damage. In *2016 IEEE Conference on Computer Vision and Pattern Recognition, CVPR 2016, Las Vegas, NV, USA, June 27-30, 2016*, pp. 2554–2564. IEEE Computer Society, 2016.
- LeCun, Y., Denker, J. S., and Solla, S. A. Optimal brain damage. In *Advances in Neural Information Processing Systems 2, [NIPS Conference, Denver, Colorado, USA, November 27-30, 1989]*, pp. 598–605. Morgan Kaufmann, 1989.

- Lee, J. H., Park, W., Mitchell, N., et al. Jaxpruner: A concise library for sparsity research. 2023.
- Li, H., Kadav, A., Durdanovic, I., et al. Pruning filters for efficient convnets. In *5th International Conference on Learning Representations, ICLR 2017, Toulon, France, April 24-26, 2017, Conference Track Proceedings*, 2017.
- Li, Y., Wei, C., and Ma, T. Towards explaining the regularization effect of initial large learning rate in training neural networks. In *Advances in Neural Information Processing Systems 32: Annual Conference on Neural Information Processing Systems 2019, NeurIPS 2019, December 8-14, 2019, Vancouver, BC, Canada*, pp. 11669–11680, 2019.
- Liu, Y., Ott, M., Goyal, N., et al. Roberta: A robustly optimized BERT pretraining approach. *CoRR*, abs/1907.11692, 2019.
- Liu, Z., Li, J., Shen, Z., et al. Learning efficient convolutional networks through network slimming. In *IEEE International Conference on Computer Vision, ICCV 2017, Venice, Italy, October 22-29, 2017*, pp. 2755–2763. IEEE Computer Society, 2017a.
- Liu, Z., Li, J., Shen, Z., et al. Learning efficient convolutional networks through network slimming. In *IEEE International Conference on Computer Vision, ICCV 2017, Venice, Italy, October 22-29, 2017*, pp. 2755–2763. IEEE Computer Society, 2017b.
- Loshchilov, I. and Hutter, F. Decoupled weight decay regularization. In *7th International Conference on Learning Representations, ICLR 2019, New Orleans, LA, USA, May 6-9, 2019*, 2019.
- Louizos, C., Welling, M., and Kingma, D. P. Learning sparse neural networks through l.0 regularization. 2018.
- Lu, L., Shin, Y., Su, Y., et al. Dying relu and initialization: Theory and numerical examples. *arXiv preprint arXiv:1903.06733*, 2019.
- Lyle, C., Rowland, M., and Dabney, W. Understanding and preventing capacity loss in reinforcement learning. In *International Conference on Learning Representations*, 2022.
- Lyle, C., Zheng, Z., Nikishin, E., et al. Understanding plasticity in neural networks. In *International Conference on Machine Learning, ICML 2023, 23-29 July 2023, Honolulu, Hawaii, USA*, volume 202 of *Proceedings of Machine Learning Research*, pp. 23190–23211. PMLR, 2023.
- Maas, A. L., Hannun, A. Y., and Ng, A. Y. Rectifier nonlinearities improve neural network acoustic models. In *in ICML Workshop on Deep Learning for Audio, Speech and Language Processing*, 2013.
- Masters, D. and Luschi, C. Revisiting small batch training for deep neural networks. *CoRR*, abs/1804.07612, 2018.
- Maxwell, J. *Theory of Heat*. Textbooks of science. Longmans, Green, and Company, 1872. ISBN 9780598862662.
- Mirzadeh, I., Alizadeh, K., Mehta, S., et al. Relu strikes back: Exploiting activation sparsity in large language models. *CoRR*, abs/2310.04564, 2023.
- Mocanu, D. C., Mocanu, E., Stone, P., et al. Scalable training of artificial neural networks with adaptive sparse connectivity inspired by network science. *Nature communications*, 9(1):2383, 2018.
- Nikishin, E., Schwarzer, M., D’Oro, P., et al. The primacy bias in deep reinforcement learning. In *International conference on machine learning*, pp. 16828–16847. PMLR, 2022.
- Oksendal, B. K. Stochastic differential equations: an introduction with applications. 6th edition. Springer Berlin, Heidelberg, 2010.
- Pillaud-Vivien, L. Rethinking sgd’s noise. <https://francisbach.com/implicit-bias-sgd/>, 2022. Accessed: 2023-08-26.
- Rachwan, J., Zügner, D., Charpentier, B., et al. Winning the lottery ahead of time: Efficient early network pruning. In *International Conference on Machine Learning, ICML 2022, 17-23 July 2022, Baltimore, Maryland, USA*, volume 162 of *Proceedings of Machine Learning Research*, pp. 18293–18309. PMLR, 2022.
- Ramachandran, P., Zoph, B., and Le, Q. V. Searching for activation functions. In *6th International Conference on Learning Representations, ICLR 2018, Vancouver, BC, Canada, April 30 - May 3, 2018, Workshop Track Proceedings*, 2018.
- Simonyan, K. and Zisserman, A. Very deep convolutional networks for large-scale image recognition. In *3rd International Conference on Learning Representations, ICLR 2015, San Diego, CA, USA, May 7-9, 2015, Conference Track Proceedings*, 2015.
- Smith, L. N. and Topin, N. Super-convergence: Very fast training of neural networks using large learning rates, 2018.
- Smith, S. L., Kindermans, P., Ying, C., et al. Don’t decay the learning rate, increase the batch size. In *6th International Conference on Learning Representations, ICLR*

- 2018, Vancouver, BC, Canada, April 30 - May 3, 2018, Conference Track Proceedings, 2018.
- Sokar, G., Agarwal, R., Castro, P. S., et al. The dormant neuron phenomenon in deep reinforcement learning. In *International Conference on Machine Learning, ICML 2023, 23-29 July 2023, Honolulu, Hawaii, USA*, volume 202 of *Proceedings of Machine Learning Research*, pp. 32145–32168. PMLR, 2023.
- Strubell, E., Ganesh, A., and McCallum, A. Energy and policy considerations for deep learning in NLP. In *Proceedings of the 57th Conference of the Association for Computational Linguistics, ACL 2019, Florence, Italy, July 28- August 2, 2019, Volume 1: Long Papers*, pp. 3645–3650. Association for Computational Linguistics, 2019.
- Trottier, L., Giguere, P., and Chaib-Draa, B. Parametric exponential linear unit for deep convolutional neural networks. In *2017 16th IEEE international conference on machine learning and applications (ICMLA)*, pp. 207–214. IEEE, 2017.
- Verdenius, S., Stol, M., and Forré, P. Pruning via iterative ranking of sensitivity statistics. *CoRR*, abs/2006.00896, 2020.
- Wang, C., Zhang, G., and Grosse, R. B. Picking winning tickets before training by preserving gradient flow. In *8th International Conference on Learning Representations, ICLR 2020, Addis Ababa, Ethiopia, April 26-30, 2020*, 2020.
- Wang, H., Zhang, Q., Wang, Y., et al. Structured pruning for efficient convnets via incremental regularization. In *International Joint Conference on Neural Networks, IJCNN 2019 Budapest, Hungary, July 14-19, 2019*, pp. 1–8. IEEE, 2019.
- Wang, H., Qin, C., Zhang, Y., et al. Neural pruning via growing regularization. In *9th International Conference on Learning Representations, ICLR 2021, Virtual Event, Austria, May 3-7, 2021*, 2021.
- Wen, W., Wu, C., Wang, Y., et al. Learning structured sparsity in deep neural networks. In *Advances in Neural Information Processing Systems 29: Annual Conference on Neural Information Processing Systems 2016, December 5-10, 2016, Barcelona, Spain*, pp. 2074–2082, 2016.
- Wojtowysch, S. Stochastic gradient descent with noise of machine learning type part I: discrete time analysis. *J. Nonlinear Sci.*, 33(3):45, 2023.
- Wolf, T., Debut, L., Sanh, V., et al. Transformers: State-of-the-art natural language processing. In *Proceedings of the 2020 Conference on Empirical Methods in Natural Language Processing: System Demonstrations*, pp. 38–45, Online, October 2020. Association for Computational Linguistics.
- Xu, B., Wang, N., Chen, T., et al. Empirical evaluation of rectified activations in convolutional network. *CoRR*, abs/1505.00853, 2015.
- Ye, J., Lu, X., Lin, Z., et al. Rethinking the smaller-norm-less-informative assumption in channel pruning of convolution layers. In *6th International Conference on Learning Representations, ICLR 2018, Vancouver, BC, Canada, April 30 - May 3, 2018, Conference Track Proceedings*, 2018.
- You, Z., Yan, K., Ye, J., et al. Gate decorator: Global filter pruning method for accelerating deep convolutional neural networks. In *Advances in Neural Information Processing Systems 32: Annual Conference on Neural Information Processing Systems 2019, NeurIPS 2019, December 8-14, 2019, Vancouver, BC, Canada*, pp. 2130–2141, 2019.



## A. Dead neurons in convolutional layers

In convolutional layers, ReLU is applied element-wise to the pre-activation feature map. We consider an individual neuron (filter) dead if all elements of the feature map post-activation are 0. Formally, in this case, the definition in Section 2.

**Definition:** The  $j$ -th neuron/filter in the convolutional layer  $\ell$  is *inactive* if it consistently outputs a feature map (post-activation) with elements summing to zero on the entire training set, i.e.  $\sum_{k,l} F_{jkl}^\ell = 0$ . A neuron/filter that becomes and remains inactive during training is considered as *dead*.

## B. Biased Random Walk Model

This section aims to illustrate the role of asymmetric noise in neuron saturation through simple theoretical models, formalizing the intuition presented in Section 2.

**Setup.** We consider a network with parameter  $\mathbf{w}$  trained to minimize the loss  $L(\mathbf{w}) = \frac{1}{n} \sum_{i=1}^n \ell_i(\mathbf{w})$ , where  $\ell_i(\mathbf{w})$  is the loss function on sample  $i$ , using stochastic gradient descent (SGD) based methods. At each iteration, this requires an estimate of the loss gradient  $g(\mathbf{w}) := \nabla L(\mathbf{w})$ , obtained by computing the mean gradient on a random minibatch  $b \subset \{1 \dots n\}$ . For simple SGD with learning rate  $\eta$ , the update rule takes the form

$$\mathbf{w}_{t+1} = \mathbf{w}_t - \eta \hat{g}(\mathbf{w}_t, b_t), \quad \hat{g}(\mathbf{w}, b) := \frac{1}{|b|} \sum_{i \in b} \nabla \ell_i(\mathbf{w}). \quad (3)$$

To formalize the intuition from section 2.1, we follow a standard line of work (Cheng et al., 2020) taking the view of SGD in Eq. 3 as a biased random walk (Anderson, 1998), described by the Langevin process,

$$\mathbf{w}_{t+1} = \mathbf{w}_t - \eta g(\mathbf{w}_t) + \sqrt{\eta} \hat{\xi}(\mathbf{w}_t, b_t) \quad (4)$$

where the zero mean variable  $\hat{\xi}(\mathbf{w}, b) := \sqrt{\eta} (g(\mathbf{w}) - \hat{g}(\mathbf{w}, b))$  represents the gradient noise. In the limit of small learning rate, Eq. 4 is also well approximated (Cheng et al., 2020, Theorem 2) by the stochastic differential equation (SDE),

$$d\mathbf{w}_t = -g(\mathbf{w}_t) + M(\mathbf{w}_t) d\mathbf{B}_t, \quad (5)$$

where  $\mathbf{B}_t$  denotes a standard Brownian motion and  $M(\mathbf{w}) := \sqrt{\mathbb{E}_b[\hat{\xi}(\mathbf{w}, b)\hat{\xi}(\mathbf{w}, b)^\top]}$ .

In SGD, a crucial characteristic of the gradient noise is its *multiplicative* nature, meaning it depends on the parameter. Systems with multiplicative noise exhibit a well-known property where regions with lower noise magnitude tend to act as attractors (Oksendal, 2010). Intuitively, the noise propels the system away from regions where it has a higher impact, leading to a higher probability of staying in regions where it has a lower impact. Mathematically, this manifests as a tendency for the invariant distribution associated with SDE in Eq. (5) to have a higher probability density in regions of lower noise magnitude.

We illustrate this phenomenon using two (drastically) simplified versions of the dynamics described by Eq. (4) and (5):

**Absorbing random walk.** We consider a one-dimensional absorbing random walk with a boundary at zero described by the SDE:

$$dw_t = \begin{cases} \sqrt{\eta} dB_t & \text{as long as } w_t > 0 \\ 0 & \text{otherwise} \end{cases} \quad (6)$$

It models a system subject to noise in an ‘active’ region  $w > 0$ , which gets stopped at 0 – and remains there, hence ‘dies’ – once it hits 0. It can be thought of as a simplified description of a regime where the dynamics (4) is dominated by noise, such as e.g., a neuron encoding features with very low correlation to the task.

The *survival probability* at time  $t$  is the probability that the system is still active  $t$ , i.e.  $w_t > 0$ . It is related to the distribution of the first hitting time at 0 of a standard Brownian motion,  $P(T_0 > t)$ , where  $T_0 = \inf\{t \geq 0 : B_t = 0\}$ . A well-known property of Brownian motion (Karatzas & Shreve, 2014) is  $\lim_{t \rightarrow \infty} P(T_0 > t) = 0$ , which shows that the system Eq. (6) eventually dies with probability 1. More generally, the following proposition specifies the dependence on learning rate and initialization:

**Proposition B.1.** Consider the system (6) initialized at  $w_0 > 0$ . The survival probability at time  $t > 0$  is given by

$$P(w_t > 0 | w_0) = \text{erf} \left( \frac{w_0}{\sqrt{2\eta t}} \right) := \sqrt{\frac{2}{\pi}} \int_0^{w_0/\sqrt{\eta t}} e^{-\frac{w^2}{2}} dw \quad (7)$$

Prop. B.1 (i) confirms that the system eventually dies almost surely, since for all  $w_0 > 0$  the survival probability decays to 0 as  $t \rightarrow +\infty$ ; (ii) implies that for any given finite horizon time  $t$ , the smaller the initialization, the more likely the system is to be dead at  $t$ , (iii) illustrates how a noisier environment (i.e. higher diffusive coefficient  $\eta$  representing the learning rate) accelerates this dying process.

*Proof.* This is a standard application of the reflection property of Brownian motions (e.g., Lawler, 2016). Let  $\bar{w}_t$  be the solution of Eq. (6) with *no* boundary condition. For the same initial condition,  $w_t$  and  $\bar{w}_t$  have the same distribution as long as  $w_t > 0$ . Let  $T_0 = \inf\{t \geq 0 : \bar{w}_t = 0\}$  be the first hitting time of  $\bar{w}_t$  at 0. The survival probability of  $w_t$  can be expressed in terms of the distribution function of  $T_0$  as

$$P(w_t > 0 | w_0) = 1 - P(T_0 \leq t) \quad (8)$$

The reflection property states that  $P(T_0 \leq t) = 2P(\bar{w}_t \leq 0)$ . To show this, let us first use the law of total probability to decompose  $P(T_0 \leq t)$  as

$$P(T_0 \leq t) = P(T_0 \leq t, \bar{w}_t \leq 0) + P(T_0 \leq t, \bar{w}_t > 0) \quad (9)$$

For the first term, we note that  $\bar{w}_t \leq 0$  implies  $T_0 \leq t$  with probability 1, so  $P(T_0 \leq t, \bar{w}_t \leq 0) = P(\bar{w}_t \leq 0)$ . For the second term, we note that by the strong Markov property,  $\bar{w}_t := \bar{w}_t - \bar{w}_{T_0} : t \geq T_0$  is a (scaled) standard Brownian motion, whose distribution is symmetric about the origin: therefore  $P(\bar{w}_t > 0 | T_0 \leq t) = P(\bar{w}_t < 0 | T_0 \leq t)$ . Thus,

$$\begin{aligned} P(T_0 \leq t, \bar{w}_t > 0) &= P(\bar{w}_t > 0 | T_0 \leq t)P(T_0 \leq t) \\ &= P(\bar{w}_t < 0 | T_0 \leq t)P(T_0 \leq t) \\ &= P(\bar{w}_t < 0, T_0 \leq t) \\ &= P(\bar{w}_t \leq 0, T_0 \leq t) \end{aligned} \quad (10)$$

where we have used the fact that  $P(\bar{w}_t = 0) = 0$ . As before, this last term equals  $P(\bar{w}_t \leq 0)$ ; and the reflection property is proved. Finally,  $d\bar{w}_t = \sqrt{\eta}B_t$  is a scaled Brownian motion with initial value  $w_0$ , so  $\bar{w}_t$  is normally distributed with mean  $w_0$  and variance  $\eta t$ . Thus,

$$P(w_t > 0 | w_0) = 1 - 2P(\bar{w}_t \leq 0) = \sqrt{\frac{2}{\pi}} \int_0^{w_0/\sqrt{\eta t}} e^{-\frac{w^2}{2}} dw$$

□

**Geometrical random walk.** The second example illustrates the stabilizing effects of multiplicative noise for systems such as Eq. (4) near unstable critical points (Oksendal, 2010). Consider the SGD dynamics (3) with a diagonal quadratic approximation of the loss around 0, i.e., we assume

$$\ell_i(\mathbf{w}) = \ell_i(0) + \frac{1}{2} \mathbf{w}^T H_i \mathbf{w}, \quad H_i = \text{Diag}(h_{i1}, \dots, h_{id}) \quad (11)$$

where  $H_i$  is some sample-dependent diagonal matrix. In such a setting, we model the dynamics of each parameter by a geometrical random walk,

$$w_{t+1} = w_t - \eta(h + \zeta_t)w_t \quad (12)$$

where  $h$  is one of the Hessian eigenvalues and  $\zeta_t$  is a noise variable sampled from some zero mean distribution. The case of a negative eigenvalue ( $h < 0$ ) is particularly interesting since it corresponds to an unstable direction (negative curvature) in the absence of noise. In what follows, to ensure the stability of the dynamics, we assume that the noise variable  $\zeta$  is bounded and the learning rate is small enough to ensure that  $\eta|\zeta| < 1$ . We also assume the noise distribution is symmetric about 0.

**Lemma B.2.** Let  $\mu = \mathbb{E}[\log(1 - \eta(h + \zeta))]$ . For all  $\epsilon > 0$  and  $\delta > 0$ , there exists  $t_0(\epsilon, \delta)$  such that for all  $t \geq t_0$ , with probability at least  $1 - \delta$ ,

$$e^{t(\mu-\epsilon)}|w_0| \leq |w_t| \leq e^{t(\mu+\epsilon)}|w_0| \quad (13)$$

In particular,  $w_t \rightarrow 0$  w.h.p whenever  $\mu < 0$ .

*Proof.* This is a consequence of the law of large numbers applied to the mean  $\bar{z}_t = \frac{1}{t} \sum_{j=0}^{t-1} z_j$  of i.i.d variables  $z_j := \log(1 + \eta(h + \zeta_j))$ : for all  $\epsilon > 0$ ,  $\lim_{t \rightarrow +\infty} P(|\bar{z}_t - \mu| < \epsilon) = 1$ . This implies that w.h.p,

$$e^{t(\mu-\epsilon)} \leq e^{t\bar{z}_t} \leq e^{t(\mu+\epsilon)} \quad (14)$$

Now solving (12) yields

$$w_t = w_0 \prod_{j=1}^{t-1} (1 - \eta(h + \zeta_j)) = w_0 \prod_{j=1}^{t-1} e^{z_j} = w_0 e^{t\bar{z}_t} \quad (15)$$

Combining with (14) proves Lemma B.2.  $\square$

**Lemma B.3.** : There exists a range of values for the learning rate  $\eta$  for which  $\mu < 0$ , making the direction stable w.h.p, despite having  $h < 0$ .

*Proof.* This is a consequence of the inequality  $\log(1 + x) \leq x - \frac{x^2}{2} + \frac{x^3}{3}$  for all  $x > -1$ . Applying this inequality to  $x = -\eta(h + \zeta)$  and taking the average over  $\zeta$  gives the upper bound

$$\mu \leq -\eta h - \frac{\eta^2}{2}(h^2 + \sigma^2) - \frac{\eta^3}{3}(h^3 + 3h\sigma^2) \quad (16)$$

where  $\sigma^2 := E[\zeta^2]$  and we used  $E[\zeta] = E[\zeta^3] = 0$  by symmetry about 0. Now, the sign of this bound coincides with the sign of the degree 2 polynomials  $P(\eta) := |h| - \frac{\eta}{2}(h^2 + \sigma^2) + \frac{\eta^2}{3}|h|(h^2 + 3\sigma^2)$ . We note that  $P(0) > 0$  and that for a small enough ratio  $|h|/\sigma$ , it has two positive roots bounding an interval on which  $P(\eta) < 0$ . One way to see this is to compute the minimum

$$\min_{\eta} P(\eta) = |h| - \frac{3}{16} \frac{(h^2 + \sigma^2)^2}{|h|(h^2 + 3\sigma^2)}, \quad (17)$$

and to observe that it goes to  $-\infty$  as  $|h| \rightarrow 0^+$  for fixed  $\sigma^2$ .  $\square$

## C. Few Dead Neurons Revive

While empirical observations have shown a gradual accumulation of dead neurons (Fig. 1), we also observed that neurons can revive (Appendix D.2). To better assess the potential impact of reviving neurons on performance, we measured the overlap ratio ( $|X \cap Y| / \min(|X|, |Y|)$ ) between the historical set of dead neurons at previous iterations and the set of dead neurons at the current iteration. This methodology directly follows Sokar et al. (2023). The results in figure 9 show that most neurons (over 90%) inactive at any point during training end up dead at the final iteration. This – coupled with our results showing that dying neurons can be dynamically pruned during training without impacting performance (Appendix F.2) – strongly suggests that neurons becoming inactive at any point during training in ReLU networks do not contribute significantly to the final performance of the trained model.

## D. Hyperparameters Impact, Additional Results

### D.1. Noise, Learning Rate and Batch Size

To investigate the role of noise, we trained a 3 layers-deep MLP (with layers of widths 100, 300, and 10 respectively) on a subset of 10 000 images of the MNIST dataset. To isolate the noise from a minibatch (of size 1) gradient ( $\hat{g}(w_j^t)$ ) we subtract from it the full gradient ( $g(w_j^t)$ ), taken over the entire training dataset. As such, the update of neuron  $j$  at every time step is given by  $w_j^{t+1} = w_j^t - \eta(\hat{g}(w_j^t) - g(w_j^t))$ .

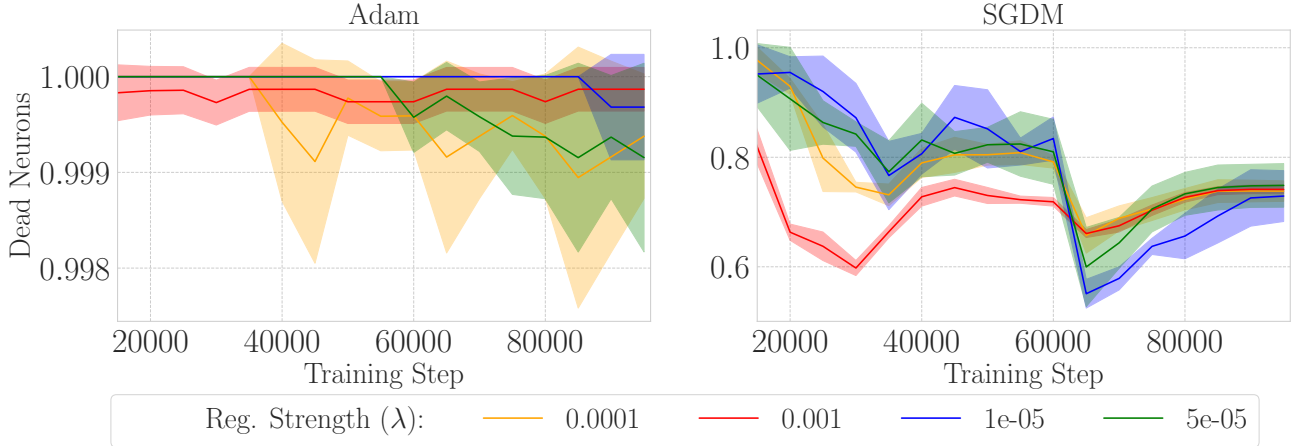


Figure 9. Overlap ratio of dead neurons during training, as measured across all layers of a ResNet-18 trained on CIFAR-10 at various maximal regularization strengths (Lasso( $\gamma$ )). Results are shown for training steps bigger than 15k when dead neurons become observable across all regularization strengths. The observation that most dying neurons remain dead justifies their early removal. **Left:** With Adam, we observe that almost all (over 99%) neurons dying never revive. **Right** The picture is more nuanced with SGDM, yet we find that the majority of dying neurons are still dead when training finishes ( $\approx 75\%$ ). Neural revival mostly happens when the learning rate is decayed, followed right after by a phase where most of the revived neurons die again.

This approach has the benefit of preserving the asymmetric noise structure of SGD updates (Wojtowysch, 2023; Pillaud-Vivien, 2022), where dead units are not affected by noise but live ones are. Compared to applying solely symmetric Gaussian noise at every time step, we notice a much sharper accumulation of dead neurons. The details are shown in Fig. 10

Diminishing the batch size or augmenting the learning rate also creates a noisier environment because both hyperparameters affect the noise covariance in SGD optimization (Keskar et al., 2017; Masters & Luschi, 2018; Goyal et al., 2017; He et al., 2019; Li et al., 2019). Furthermore, Smith et al. (2018) shows that learning rate decay can be replaced with batch size growth, emphasizing the relationship between the two quantities. Because of their impact on noise, we should expect those quantities to affect the dying ratio of neurons. We confirm empirically this hypothesis in Fig. 11.

## D.2. Training Time

The relation with training time, asserting that the probability of a neuron dying increases as training progresses (Prop. B.1) doesn’t entirely align with practical applications. Modern overparameterized architectures often can memorize the entire training dataset, achieving zero loss in the process. Given that the gradient signal is proportional to the loss, it would concurrently diminish to zero for all neurons, preventing any further death.

We observe a pattern consistent with this idea (Fig. 1), where the total count of dead neurons spikes sharply in early training to then fluctuate slightly before stabilizing. The fluctuations demonstrate that neurons *can indeed revive*. However, additional experiments with ReLU networks revealed that most reviving neurons die again later (Fig. 9) and that their dynamic elimination has negligible to no impact on performance (Fig. 8).

## D.3. Network Width

The widths of a neural network’s layers also influence the ratio of live neurons (live neurons to total neurons in the network) post-training (see figure 11). Typically, this ratio increases with the width; however, the total number of live neurons continues to rise with increased width. This phenomenon is somewhat anticipated as incorporating more neurons with random initialization in any given layer can only amplify the training noise, especially in the initial phase. Moreover, since initialization functions usually adjust their standard deviation proportionally to the number of channels ( $\sigma \propto \sqrt{\frac{1}{\text{fan\_in} + \text{fan\_out}}}$ ), widening the network places neurons closer to their inactive region right from the initialization. The connection between width and dead neurons maintains its significance as neural network sizes are inclined to increase over time with the availability of more computational resources. If this trend persists, the accumulation of dead neurons could potentially



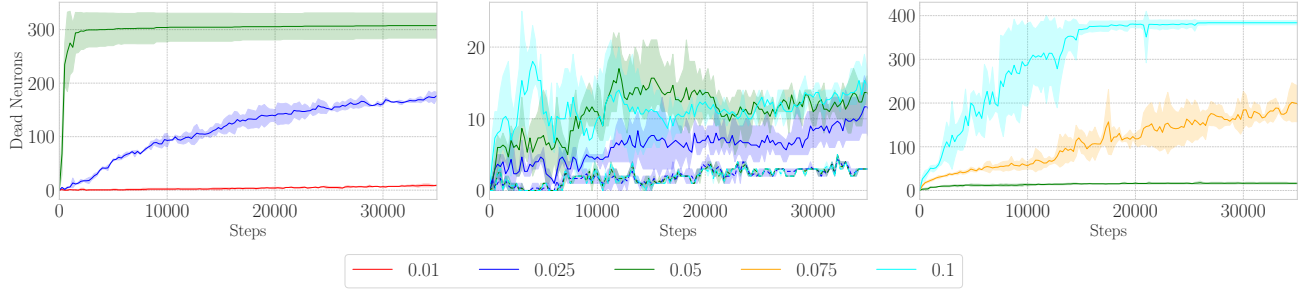


Figure 10. Evolution of the number of dead neurons for a 3-layer MLP (with layers of widths 100, 300, and 10 respectively) on a subset of MNIST. **Left:** The noisy part of the minibatch gradient is isolated and used exclusively to update the parameters. Noisy updates are *sufficient* to kill a subset of neurons following standard initialization. Because SGD gradient is 0 for dead neurons, there is an **asymmetry**: only live neurons are subject to noisy updates. **Center:** Gaussian noise is added to the parameters update, either asymmetrically (applied only to live neurons, plain lines) or symmetrically (dashed lines). Asymmetric noise is much more prone to dead neuron accumulation while symmetric Gaussian noise can revive neurons, contrary to SGD noise, leading to a much smaller accumulation. **Right** Standard SGD. Dead neurons accumulate quickly in noisy settings, but they plateau when the NN converges (leading to zero gradient). Results are averaged over 3 seeds.

become increasingly pervasive.

## E. Adam is a Neuron Killer

The greater impact of Adam over the dying ratio compared to momentum must be due to the second-moment term, which is the only significant difference with momentum. Recall that Adam update is (Kingma & Ba, 2015):

$$\begin{aligned} m_t &= \beta_1 \cdot m_{t-1} + (1 - \beta_1) \cdot g_t \\ v_t &= \beta_2 \cdot v_{t-1} + (1 - \beta_2) \cdot g_t^2 \\ \hat{m}_t &= \frac{m_t}{1 - \beta_1^t} \\ \hat{v}_t &= \frac{v_t}{1 - \beta_2^t} \\ \theta_{t+1} &= \theta_t - \frac{\eta}{\sqrt{\hat{v}_t} + \epsilon} \cdot \hat{m}_t \end{aligned}$$

Earlier, we hypothesized that the neurons ending up dead were the ones experiencing very small gradients, such that the noise dominated their update trajectories. If this is the case,  $g_t^2$  (the squared gradient) would be very small for those neurons’ parameters, eventually leading to a very small second-moment estimation  $\hat{v}_t$ . In such a scenario,  $\epsilon$  would end up dominating  $\sqrt{\hat{v}_t}$ , effectively multiplying the learning rate by  $\epsilon$  which is typically set to  $1 \times 10^{-8}$ . Moreover, as the decay ( $\beta_2 = 0.99$ ) of  $\hat{v}_t$  is usually slower than the one of  $\hat{m}_t$  ( $\beta_1 = 0.9$ ), a few sudden noisier updates would be sufficient to make huge random steps.

It is worth noting that RL practitioners typically set epsilon to a higher value (Hessel et al., 2018), as it has empirically been found to perform better. Higher  $\epsilon$  values should reduce the number of dead neurons induced by Adam optimizer, which could be the cause for the improved performance/stability observed in RL. Also, because of constant distribution shifts, rapid accumulation of dead neurons often occurs in RL tasks.

Also notable, HuggingFace Transformers library (Wolf et al., 2020) default  $\epsilon$  Adam parameter to  $1 \times 10^{-6}$ , following RoBERTa example (Liu et al., 2019). Manipulating the  $\epsilon$  parameter of AdaGrad was also observed to impact significantly a transformer performance model (Agarwal et al., 2020). Verifying if those heuristic choices are due to their impact on dead neuron accumulation would be quite interesting.

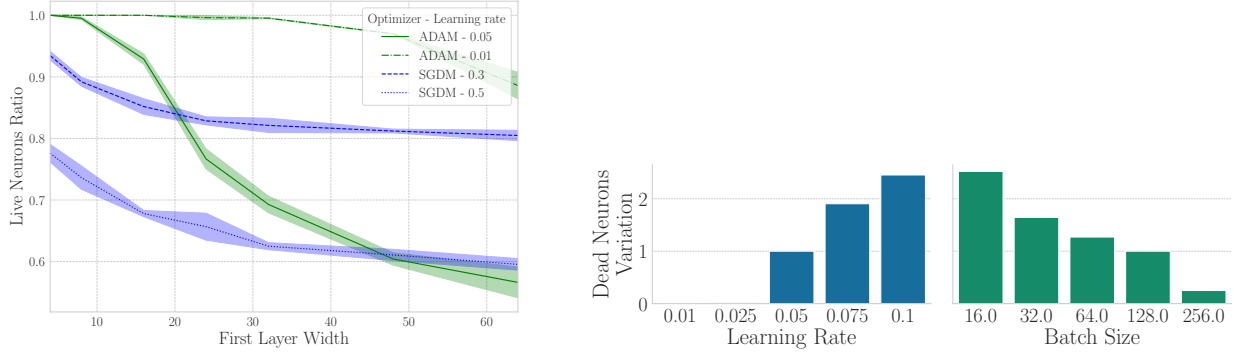


**Figure 11. Left:** An increased width leads to a higher ratio of neurons dying, independently of the optimizer. Measured on a ResNet-18 trained on CIFAR-10, without added regularization, across 3 seeds. We use the number of channels in the initial layer of the ResNet-18 to indicate the width, with 64 being the number of channels proposed by He et al. (2016) for the first convolution layer. **Right:** Varying the hyperparameters of a ResNet-18 (CIFAR-10) impacts the number of dead neurons. The bar heights indicate the multiplicative ratio of dead neurons compared to the base configuration ( $lr = 0.05$ ,  $bs = 128$  and  $\lambda = 0$ ). The number of training steps was kept **constant** when varying the batch size for fair comparisons. Quantities are averaged over 3 random seeds.

## F. Pruning Method Ablation

We validate and justify the heuristic choices made for our pruning method via empirical observation exposed in this section. We used the same setup as before for a ResNet-18 trained on CIFAR-10.

### F.1. Regularizer choice

In our empirical analysis, we evaluated the effectiveness of various regularizers on the performance of ResNet-18 networks trained on CIFAR-10, using either Adam or SGDM as optimizers. Our findings (Fig. 6) suggest that focusing regularization exclusively on scale parameters yields a more favorable balance between sparsity and performance with both optimizers. While L2 regularization on scale parameters slightly enhances performance, the scenario changes with SGDM, where Lasso regularization on these parameters outperforms others by a wider margin. Consequently, for the sake of simplicity in our experiments, we have chosen to consistently apply Lasso regularization to scale parameters.

### F.2. Dynamic Pruning

To verify the impact of dynamic pruning, we measured if there were any performance discrepancies when it was enabled or not. Across runs, we varied the regularization strength while measuring accuracy and sparsity. The results, in Fig. 8, show that enabling dynamic pruning does not affect the final performance. The very slight variations between runs fall well between the expected variance across different runs. This experiment reinforces the hypothesis that neurons that die and later revive during training do not contribute significantly to the learning process.

### F.3. Dead Criterion Relaxation

To measure if a minibatch could be used to measure the death state instead of the entire dataset, we tracked the number of dead neurons during training with both metrics in Fig. 12. We used a minibatch containing 512 inputs from the training dataset for the proxy measurement. We can see that both curves closely track each other. More importantly, they match at the end of the training, indicating that overall the same amount of neurons would be removed when performing the death check over the minibatch. Dynamic pruning was disabled for this experiment.

### F.4. Regularization Schedule

We also empirically tested different schedules over the regularization parameter in Fig. 5, trying to mitigate the impact of high regularization by decaying the parameter throughout the training after a warmup phase. We settled on using a one-cycle scheduler for the regularization strength because of slightly better performance in the higher sparsity level. However, we remark that all tested schedules over the regularization parameter remain sound with our method.

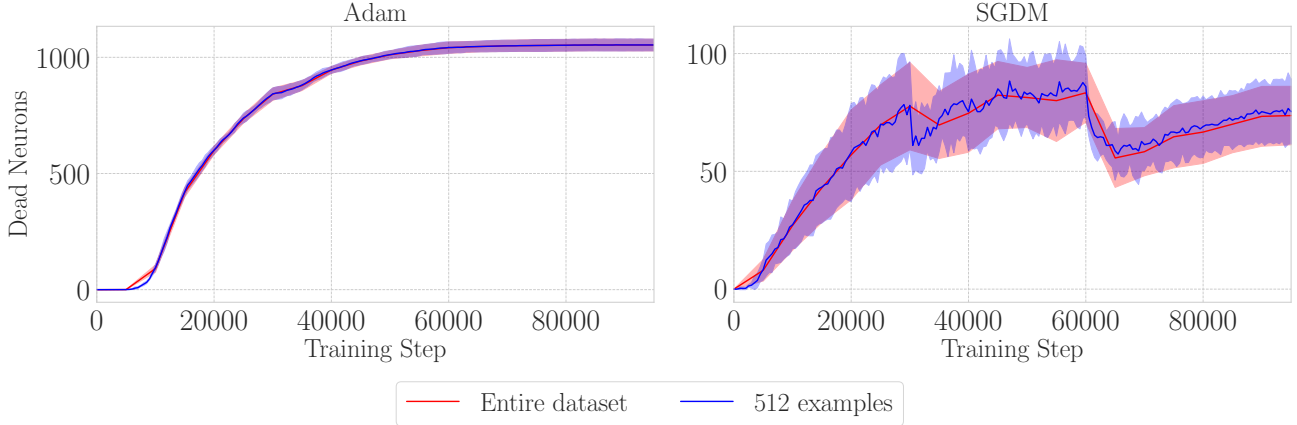


Figure 12. Instead of validating the death state of neurons against the entire training dataset, it proves sufficient to use a smaller dataset. The curves match throughout training, indicating that roughly the same number of neurons are removed with both strategies. Experiments were performed with ResNet-18 and Lasso( $\gamma$ ) regularization on CIFAR-10 for 3 seeds. **Left:** With Adam. **Right:** With SGDM.

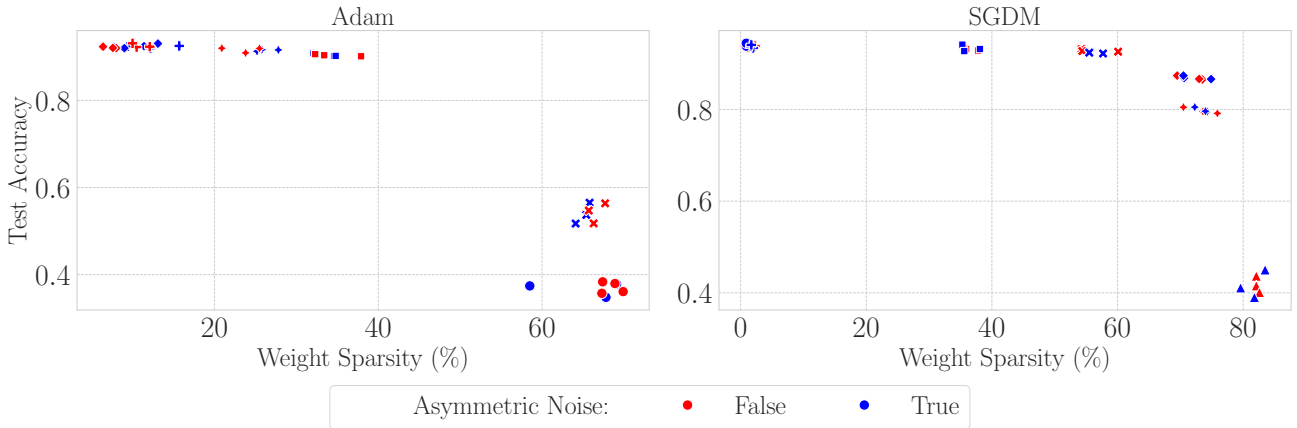


Figure 13. Weight sparsity for a ResNet-18 trained on CIFAR-10 while varying the variance of the added noise, *without adding any regularization*. The experiments were made with dynamic pruning enabled and showcased that using asymmetric noise over the live neurons only instead of symmetric noise across neurons does not impact the tradeoff. **Left:** With Adam, **Right:** With SGDM.

## F.5. Added Noise

We measured empirically the impact of adding artificial asymmetric noise. As expected, adding too much noise hurts performance. However, when noise variance is small enough, it doesn’t affect performance while helping neurons to cross over in the inactive region, as detailed in Fig. 7. The effect is particularly significant when training a ResNet-50.

Furthermore, we assess that increasing noise instead of regularization is also a valid strategy for pruning, as showcased in Fig. 13. However, it leads to a worse tradeoff than when using increased regularization. Significantly, in this setting, with dynamic pruning enabled, we notice no major difference in performance between using asymmetric or symmetric noise.

## G. Additional Results

We report additional results in this section, including the pruning performance of DemP when pruning a VGG-16 (Fig. 14) trained with both Adam and SGDM and when pruning a ResNet-50 trained with SGDM (Table 3). Results are similar, with DemP outperforming baselines with Adam at high sparsity. However, the performance of DemP with SGDM decay abruptly passed 95% weight sparsity, which may be due to improper tuning of the method when using a one-cycle learning scheduler to train for a small number of epochs (see Appendix H.2). The results with Leaky ReLU are in Fig. 15.

We included results from Lee et al. (2023) and Evci et al. (2020) in Table 3 to better illustrate the trade-off between structured

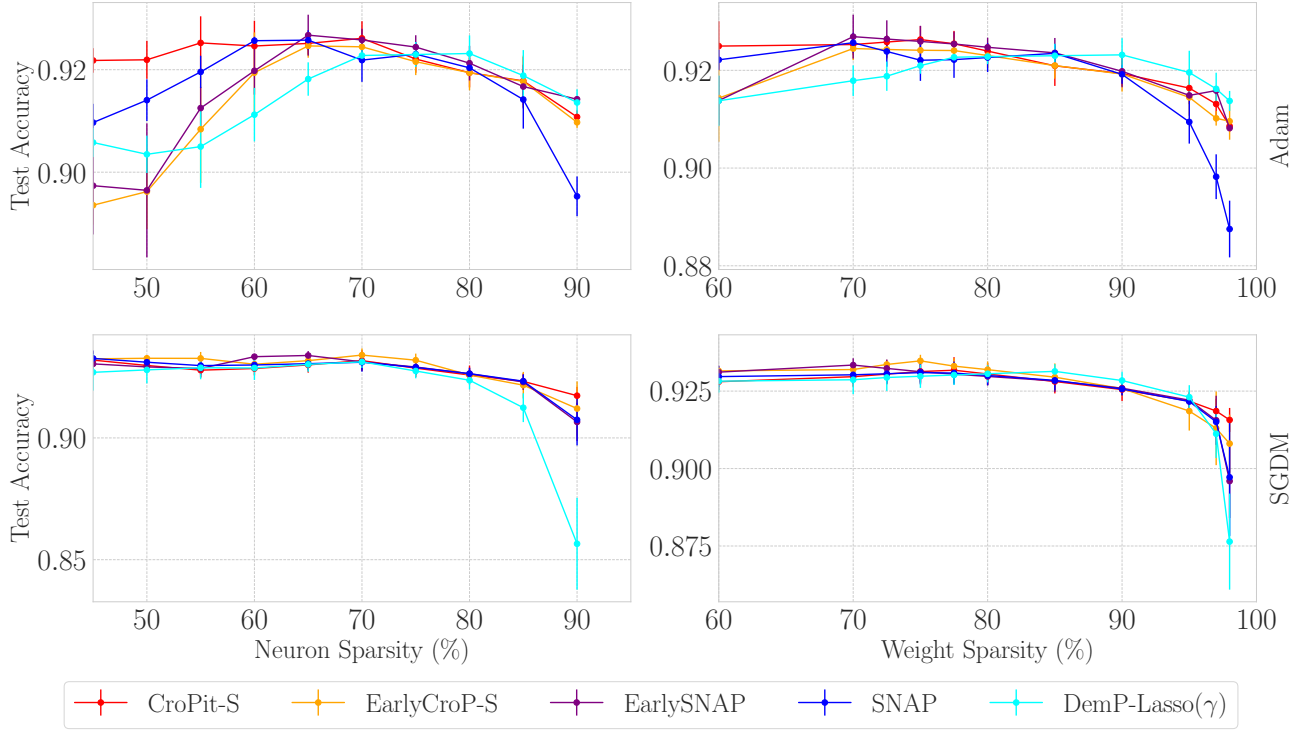


Figure 14. The results on VGG-16 networks trained with Adam (**Top**) and SGDM (**Bottom**) on CIFAR-10. With Adam at high sparsities, DemP can find subnetworks that better maintain performance. With SGDM, the performance instead decays quickly compared to baseline when reaching  $\approx 95\%$  weight sparsity ( $\approx 80\%$  neural sparsity). Higher sparsities with DemP are obtained by increasing the peak strength of the added scheduled regularization. **Left:** Neural sparsity, structured methods. **Right:** Weight sparsity, structured methods.

and unstructured pruning methods. While unstructured methods currently offer more potential to maintain performance at higher parameter sparsity, structured methods offer direct speedup advantages.

### G.1. Comparison with Unstructured Methods

We employ the `JaxPruner` package (Lee et al., 2023) to illustrate further trade-off of our method against some unstructured methods. Our method is capable of achieving *similar* performance to unstructured ones for the ResNet-18 experiments (Fig. 16). The comparisons with the unstructured methods use their default configuration from JaxPruner, which was tuned for a ResNet-50. We expect their performance on smaller models to be improved by tuning the pruning distribution, the pruning schedule, and the pruning iterations scheme (Lee et al., 2023). However, for those not interested in expensive tuning, our method becomes an interesting default choice.

## H. Implementation details

### H.1. ResNet-18/ResNet-50

We mostly followed the training procedure of Evci et al. (2020) for the ResNet architectures.

**ResNet-18.** We train all networks for 250 epochs using a batch size of 128. The learning rate is initially set to 0.005 for Adam, to 0.1 for SGDM, and is thereafter divided by 5 every 77 epochs. While varying regularization is used with our method, it is on top of a constant weight decay (0.0005) used across all methods, including ours. Random crop and random horizontal flips are used for data augmentation.

**ResNet-50.** We trained the ResNet-50 for 100 epochs, with a batch size of 256 instead of 4096. The initial learning rate is set to 0.005, before being decayed by a factor of 10 at epochs 30, 70, and 90. Label smoothing (0.1) and data augmentation (random resize to either  $256 \times 256$  or  $480 \times 480$ , before randomly cropping to  $224 \times 224$ . Followed by random horizontal flip and input normalization) are also used. We again use Adam and SGDM, using constant weight decay (0.0001) for both.



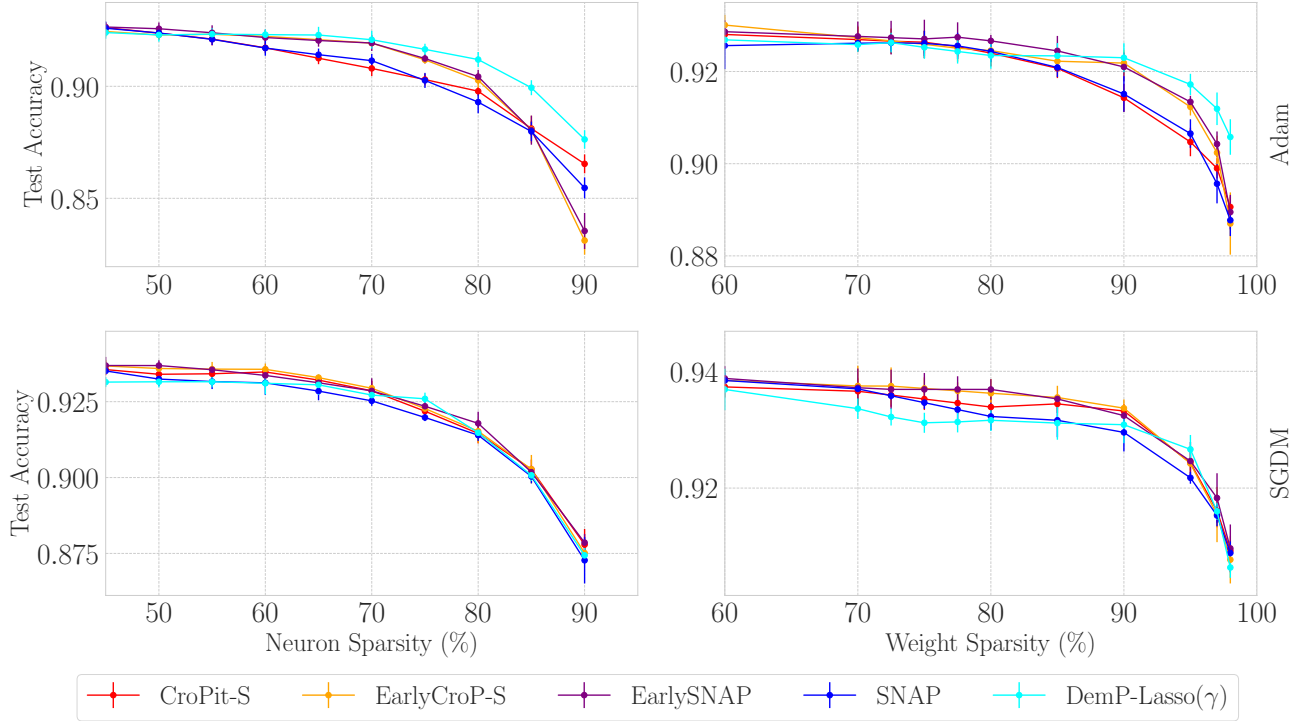


Figure 15. **Top:** ResNet-18 networks with *Leaky ReLU* trained on CIFAR 10 with Adam. DemP again outperforms the baseline structured pruning methods when using Adam. Higher sparsities with DemP are obtained by increasing the peak strength of the added scheduled regularization. **Bottom:** With SGDM, DemP performance is again similar to other methods. **Left:** Neural sparsity, structured methods. **Right:** Weight sparsity, structured methods.

## H.2. VGG-16

We followed a training procedure similar to [Rachwan et al. \(2022\)](#). We used Adam and SGDM with respectively a learning rate of 0.005 or 0.1 and a batch size of 256, with the One Cycle Learning Rate scheduler ([Smith & Topin, 2018](#)). The networks are trained for 80 epochs. CIFAR-10 images are normalized and resized to  $64 \times 64$  before applying random crop and random horizontal flip for data augmentation.

## H.3. Structured Methods

We closely reimplement in JAX ([Bradbury et al., 2018](#)) the structured methods from [Rachwan et al. \(2022\)](#), keeping all the hyperparameters specific to every method as is. The training hyperparameters are the same as specified in [H.1](#) and [H.2](#).

## H.4. Unstructured Methods

For the unstructured methods, we rely on [Lee et al. \(2023\)](#) implementations, using their method’s configuration for pruning a ResNet-50 for all our experiments. The training hyperparameters are the same as specified in [H.1](#) and [H.2](#).

Table 3. Comparison between different criteria when pruning a ResNet-50 trained on ImageNet with SGDM around 80% (first line) and 90% (second line) weight sparsity. Similarly to what was observed in smaller models, DemP performs similarly to top baselines, outperforming EarlyCrop here by a small margin. Because structured pruning methods do not have precise control of weight sparsity, we report the closest numbers obtained to these target values.  $\pm$  indicates the standard deviation, computed from 3 seeds. The sparsity numbers indicate the removed ratio.

	Method	Test accuracy	Neuron sparsity	Weight sparsity	Training time	Training FLOPs	Inference FLOPs
Structured	Dense	74.98% $\pm 0.08$	-	-	1.0x	1.0x (3.15e18)	1.0x (8.2e9)
	SNAP	26.05% $\pm 0.17$	36.90%	81.40%	0.54x	0.33x	0.33x
		24.84% $\pm 0.11$	56.07%	90.10%	0.47x	0.25x	0.25x
	CroPit-S	25.93% $\pm 0.06$	36.90%	81.40%	0.50x	0.31x	0.31x
		25.44% $\pm 0.05$	53.20%	89.80%	0.49x	0.26x	0.26x
	EarlySNAP	70.06% $\pm 0.16$	38.73%	79.97%	0.87x	0.57x	0.56x
		64.25% $\pm 0.10$	57.23%	89.73%	0.78x	0.44x	0.44x
	EarlyCroP-S	71.45% $\pm 0.29$	41.13%	79.77%	0.86x	0.61x	0.61x
		67.04% $\pm 0.18$	58.77%	90.07%	0.80x	0.48x	0.48x
	DemP-Lasso( $\gamma$ )	<b>72.21%</b> $\pm 0.19$	<b>53.50%</b>	79.43%	0.88x	0.62x	0.58x
		<b>67.76%</b> $\pm 0.12$	<b>68.51%</b>	89.73%	0.69x	0.46x	0.41x
	Dense <sup>†</sup>	76.67%	-	-	-	-	-
	Dense*	76.8 $\pm 0.09$ %	-	-	-	1.0x (3.2e18)	1.0x (8.2e9)
Unstructured	Mag <sup>†</sup>	<b>75.53%</b>	-	80%	-	-	-
	Sal <sup>†</sup>	74.93%	-	80%	-	-	-
	SET*	72.9% $\pm 0.39$	-	80%	-	0.23x	0.23x
		69.6% $\pm 0.23$	-	90%	-	0.10x	0.10x
	RigL (ERK)*	75.10% $\pm 0.05$	-	80%	-	0.42x	0.42x
		<b>73.00%</b> $\pm 0.04$	-	90%	-	0.25x	0.24x

<sup>†</sup> values obtained from Lee et al. (2023)

\* values obtained from Evci et al. (2020)

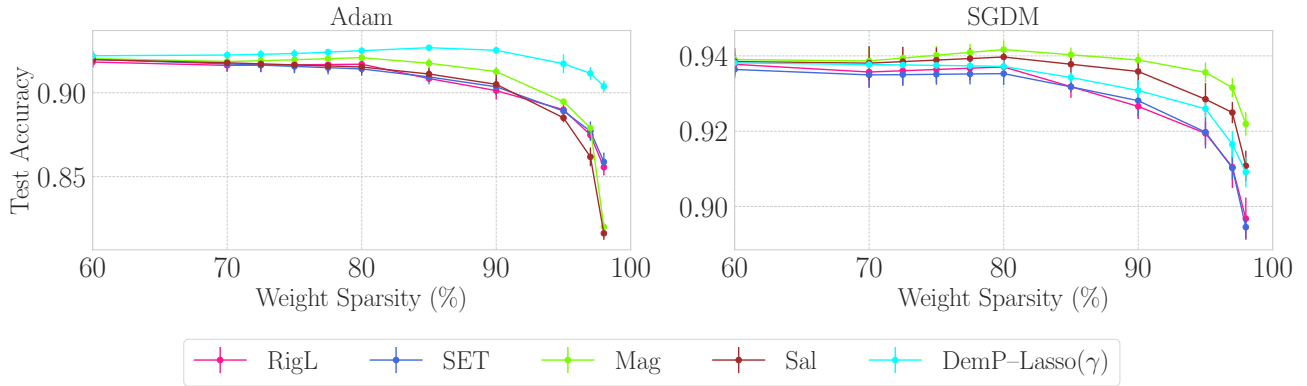


Figure 16. Comparison between DemP and unstructured pruning methods from Lee et al. (2023), performed on ResNet-18 trained on CIFAR-10 over 3 seeds. Higher sparsities with DemP are obtained by increasing the peak strength of the added scheduled regularization. **Left:** With Adam, DemP proves more effective than the unstructured methods left at their base configuration, even if it cannot achieve the same granularity in sparsity by being a structured method. **Right:** With SGDM, DemP performs similarly.